2018

Depairing current density in NbTiN superconducting films

Nahid Shayesteh Swails
University of South Carolina

Depairing current density in $NbTiN$ superconducting films

by

Nahid Shayesteh Swails

Bachelor of Arts
Isfahan University of Technology 2005

Master of Science
Shahrekord University 2008

Submitted in Partial Fulfillment of the Requirements

For the Degree of Doctor of Philosophy in

Physics

College of Arts and Sciences

University of South Carolina

2018

Accepted by:

Milind N.Kunchur, Major Professor

Richard Creswick, Committee Member

Yanwen Wu, Committee Member

Maksymilian Chruszcz, Committee Member

Cheryl L. Addy, Vice Provost and Dean of the Graduate School

Dedication

I dedicate this thesis to my beloved husband:

Richard Arthur Swails

And my entire family

Acknowledgments

Upon the completion of this manuscript I am grateful to many people. I owe a debt which cannot be repaid to my family, who have cultivated and constantly nurtured a love for the acquisition of knowledge, and without whose support I would not be writing this preamble. Their selfless sacrifice and the prayers of my entire family have culminated in this thesis. I am deeply grateful for the guidance, support, and care shown to me by my adviser Professor Milind Kunchur. He has never faltered in his enthusiasm for this work, and has taught me many valuable lessons. I am happy to have had the opportunity to explore the world of physics under his direction. I am thankful to the entire faculty of the physics department who have always been willing to help in small and large matters. I wish to thank the members of my dissertation committee: Richard Creswick, Yanwen Wu and Maksymilian Chruszcz for generously offering their time, support, guidance and good will throughout the preparation and review of this document. I would especially like to express my gratitude to my fellow graduate student Charles Dean who provided crucial and significant assistance with various aspects of this research. I also thank my office-mate Stacy Varner for all his help and support. I have made many friends in the physics department over the years, and I thank them all for their friendship and assistance. For a complete set of acknowledgments, many pages would be needed as the number of people who have assisted me is large. I apologize to those I have not mentioned above in the interest of brevity. Your help has not gone unappreciated, and my well wishes are with you.

Abstract

In this work, we systematically investigate the superconducting properties of Niobium Titanium Nitride ($NbTiN$) superconducting films with different geometries, which at low temperature remain superconducting. $NbTiN$ superconducting films with a few nm thickness are widely used in devices such as superconductor-insulator-superconductor (SIS) mixers, superconducting cavities and resonators and superconducting nanowire single-photon detectors ($SNSPD$). In all these applications, films of varying dimensions are required to achieve optimal performance. The initial thickness of our samples was 125 nm deposited on a silicon substrate. We change the thickness of our samples using lithography and ion milling. We measure and analyze the thickness dependence of various superconducting properties of these films.

Table of Contents

List of Tables

List of Figures

Introduction

In 1911, Dutch physicist Heike Kamerlingh Onnes observed superconductivity for the first time in mercury, while studying the electrical properties of different types of materials at cryogenic temperature. He witnessed that the electrical resistance of mercury disappears at around 4.2 K which is very close to absolute zero temperature. Later on, he reversed the process and observed that at around 4.2 K, resistance goes back in the material. This transition temperature is called critical temperature (T_c) and depends on the type of superconducting material can be different. He called this phenomenon superconductivity and he won the Nobel Prize of Physics is 1913 for this discovery. Since that time, lots of other superconducting materials have been discovered and the theory behind this subject also has been developed to a large extent. Superconductors have applications in different sectors like high energy physics, electric power, medicine, transportation, electronic/communication, defense/space and industrial equipment [3] [1] [14].

In 1933, Walther Meissner and Robert Ochsenfield [37] observed that superconducting materials expel magnetic field during their transition to the superconducting state. In their experiment, they cooled down tin (Sn) and lead (Pb) samples below their critical temperature. They observed, almost all of the interior magnetic field was canceled. Due to the fact that magnetic field flux in a superconductor is conserved, they observed an increase in the exterior field. The state in which a superconductor has a little or no magnetic field inside itself is called Meissner state. In this state, superconductors exhibit perfect diamagnetism which sometimes is called supermagnetism. Supermagnetism breaks down by increasing the applied magnetic field and

this transition magnetic field is called critical magnetic field (B_c).

In 1986, Bednorz and Muller [8] published an article called "Possible high T_c superconductivity in the $Ba - La - Cu - O$ system" that revitalized the subject of superconductivity. They discovered a new class of materials with unexpected high critical temperature, called cuprates superconductors. These types of material have CuO_2 planes which are believed to dominate the properties of them.

The microscopic theory of superconductivity by Bardeen, Cooper and Schrieffer (BCS) [6] is widely used to interpret superconductivity. In this theory, the electrons condense into pairs and those pairs are current carriers. The binding of these pairs is because of the electron-phonon interactions inside the superconductor. For the temperatures close to T_c, the phenomenological Ginzburg-Landau theory (1950), can be used because it is handled easier, also it can be derived from the BCS formalism. However, it is still controversial whether the BCS theory work well in the high temperature superconductors or not. Researchers are recently interested in the development of a new non-BCS theory.

In 1998, Stern et al. [42] made Niobium Titanium Nitride ($NbTiN$) films by reactive DC-magnetron sputtering method. $Nb - Ti$ alloy target has been used in a mixture of Argon and Nitrogen atmosphere. They had difficulties with impurities of metal in some of their targets. For getting better quality films, they used X-ray photoemission spectroscopy in their deposition system. They have used different films in which the portion of Nb to Ti weight was kept 78% to 22%. They were interested in RF-losses (Radio Frequency losses) of those films in terahertz frequency range. For that purpose they needed films with the energy gap higher than 2.5 meV. In order to achieve that, they made their films with critical temperature higher than $15K$. They also noticed, better quality films have lower resisttivity above T_c. They observed for frequencies below 1 THz, $NbTiN$ has very low RF-losses.

For receivers in millimeter and submillimeter radio astronomy, superconductor-

insulator-superconductor (SIS) mixer is an important element. In radio astronomy, the electromagnetic spectrum of astronomical objects at really high radio frequencies (RFs) is one of the main area of different studies. For this specific application, mixers with lowest possible noise are proffered. That is the main reason that nowadays SIS mixers are widely used rather than Schottkey diode ones. For making a sensitive SIS mixer to incoming radiation, well coupled SIS junctions are necessary. In SIS junction which is one type of Josephson junction, due to quantum tunneling, current passes through that junction and across that junction current flows without any voltage applied until maximum critical current is reached. Radio frequency waves of frequency f, irradiate from Josephson junction and because of that the frequency of microwave can be determined accurately [40].

$NbTiN$ is a material with almost high T_c as Niobium Nitride (NbN), but higher quality and lower resistivity. The properties of $NbTiN$ films were investigated for the first time around the time that NbN films were fabricated. In 1999, $NbTiN$ based, low noise, high frequency (SIS) mixer was fabricated by Kawamura et al. [18]. In their mixer, they used an interlayer of Au between $NbTiN$ plane and Nb base. The sensitivity of their mixer was almost twice as Nb based one, which was made right before this one (in the same frequency range (850 GHz).

$NbTiN$ has a theoretical energy gap of $\sim$ 1.7 times of NbN, which makes it having low loss in frequency range up to 1.2 GHz. Cecil et al. [9] made $NbTiN$ films with resistivities in a range from 50 μ-ohm-cm to 150 μ-ohm-cm depending on the deposition condition. The quality of their films, depended on ratio of N_2 to Ar and also deposition rate. They claimed for films with lower resistivity and higher comprehensive stress, sputtering should be done in lower pressure ($\sim$ 4-6 m $torr$). They have used ellipsometry for evaluation of optical properties of $NbTiN$ films. They reported changing in the optical properties is reflecting the change in the resistivity and T_c.

$NbTiN$ is widely used in RF cavities for particle accelerators, hot electron bolometer (HEB) mixers, coplanar waveguide superconducting resonators and superconducting nanowire single photon detectors ($SNSPD$). For Superconducting nanowire Single photon detectors, $NbTiN$ films with high Ti composition were made by Jia et al. [17]. $NbTi$ alloy target used in DC reactive sputtering machine was 47% Ti and 53% Nb in ambient temperature. Ar to N_2 ratio was 1 to 5 and they were optimized at 1.5 m $torr$ pressure. The current was 0.7 A and the thickness of the film was controlled accurately. They observed by increasing Ti composition in their films, T_c and resistivity are decreasing.

Superconducting films used at phonon-cooled hot electron bolometer (HEB) mixers, should be thin (a few nm only) for hot electrons to cool down fast and efficient. Shiino et al. [41] observed that $NbTiN$ films have higher T_c (16 to 18 K) and lower resistivity in bulk, but lower T_c and higher resistivity in the case of thinner films. For good quality HEB mixers, higher T_c films are preferred. In order to obtain high quality thin films, they used epitaxial growth on substrate. For that purpose, both lattice structure of film and substrate should match. This means the choices for substrate are limited to big extent. One method to improve lattice matching is to heating the substrate and the other one is to use a buffer layer between film and substrate. For their $NbTiN$ films with quartz or soda glass substrate, they used AIN layer in between.

For photon detection applications, superconducting resonators have been widely used. Temperature and noise dependent resonance frequency was measured in $NbTiN$ superconducting resonators that are covered with different thickness of SiO_x by Barens et al. [7]. They noticed that when resonators are covered by SiO_x, noise jumps to a higher level, independent of the layer thickness. They also observed the resonance frequency deviations are depending on temperature and the volume of SiO_x.

In the superconducting state, disorder does not affect the properties of superconductors. Therefore, it is expected for superconducting films to have a fixed T_c independent of disorder. This can be explained by quasiparticle density of states and BCS gap. Driessen et al. [11] observed that for superconductors with resisitivity higher than 100 $\mu\Omega$ cm, the theory revealed severe deviation. Numerical simulations showed that by increasing the disorder, eventually inhomogeneous superconducting state will rise (even for homogeneous disorder). A series of TiN and $NbTiN$ films with different normal resistance and different resistivity (ranging from 120 to 150 $\mu\omega$cm) were made by them. The more they increased the disorder, they saw more deviation from BCS theory. Their hypothesis was that those deviations are because of short elastic scattering length in their films.

In 2015, high quality $NbTiN$ films of different thickness were fabricated by Zhang et al. [46]. Epiataxiail $NbTiN$ films were deposited on a single-crystal MgO substrate. They were able to change the composition of their films by changing the deposition conditions. In all their films, $NbTiN$ had a uniform composition. A lot of superconducting devices, require ultrathin films of the order of nanometers. However, NbN thin films are well known for their superconducting properties highly depending on the thickness and substrate. The variation in the composition and crystality is depending on the thickness of the film and type of the substrate. Compare with NbN, the superconducting and electrical properties of $NbTiN$ films are less substrate dependent. In addition to electrical properties, their chemical properties might also change depending on the thickness. The observed, T_c was gradually decreasing by the decrease of the thickness. For the thickness less than 10 nm, the electrical properties (T_c and residual-resistivity ratio) dropped suddenly. They concluded, for fabricating a high quality thin film, deposition parameters should be optimized point by point.

Chapter 1

Theories of Superconductivity

London equations

Brothers F. and L. London [34] for the first time were able to interpret Meissner effect by building up a relationship between magnetic field B, current density j and electric field E in the superconducting materials. Their assumption was that in an electric field, electrons experience no friction, so the equation of motion in an electric field and the current density will be:

$$m_e \frac{\partial v}{\partial t} = -eE \tag{1.1}$$

$$j = en_s v \tag{1.2}$$

here e is the charge of the electron, v is speed of an electron, m_e is electron mass and n_s is superconducting electron density [12]. Therefore:

$$\frac{\partial j}{\partial t} = \frac{n_s e^2}{m_e} E \tag{1.3}$$

by taking the derivative of current versus time and substituting it in Eq.1.1, we can get to the first equation that London brothers proposed. This equation shows that the current inside a superconductor is changing because of the fact that electrons accelerate by the electric field. The value of electric field E:

$$E = \mu_0 \lambda_L^2 \frac{\partial j}{\partial t} \tag{1.4}$$

where,

$$\lambda_L = \sqrt{m_e / \mu_0 n_s e^2} \tag{1.5}$$

is London penetration length. This is a distance in which the magnetic field penetrates into a superconductor and becomes equal to e^{-1} times that of the magnetic field at the surface of the superconductor. λ_L is usually in the order of $10^{-6}m$ and is depending on the temperature close to T_c. By using Maxwell equation $\nabla \times E = -\frac{\partial B}{\partial t}$ and taking curl of Eq.1.4, we get to:

$$\frac{\partial}{\partial t}(\frac{m_e}{n_s e^2}\nabla \times j + B) = 0 \tag{1.6}$$

Because the derivative in this equation is equal to zero, the quantities in parenthesis are equal to a constant value. In London brothers assumption, the constant value is equal to zero. Therefore:

$$\nabla \times j = -\frac{n_s e^e}{m_e}B \tag{1.7}$$

where gives us the second equation proposed by London brothers:

$$B = -\mu_0 \lambda_L^2 \nabla \times j \tag{1.8}$$

the second equation can be manipulated by Maxwell's equation $\nabla \times B = \mu_0 j$ in the form of:

$$\nabla^2 B = \frac{B}{\lambda_L^2} \tag{1.9}$$

The solution to this equation for a special case in which B changes only in the z direction, will be $B = B_0 e^{-z/\lambda_L}$. This equation is able to explain Meissner effect to great extent. Except for the thicknesses in the order of λ_L, the magnetic field does no penetrate inside the superconductor. This equation shows that B is not uniform and has exponential decay. It also shows that the nature of decay depends on the superconducting electron density (n_s). λ_L is usually in the order of micrometer and is temperature dependent. The temperature's dependence of λ_L close to T_c is shown empirically to be:

$$\lambda_L(T)^{-1} \approx \lambda_L(T)^{-1}\sqrt{1-(t)^4} \tag{1.10}$$

where, $t = T/T_c$.

The superconducting phase

There is a phase transition for a material form the normal to the superconducting state when it cooles down below T_c and also when the magnetic field decreases to magnetic fields lower than B_c [36]. Gibbs free energy equation in the presence of magnetic field based on classical thermodynamic is:

$$G = U - TS - M.B \tag{1.11}$$

where internal energy of superconductor is shown by U, the entropy by S and magnetization by M (magnetic moment per unit volume). Its differential equation then will be:

$$dG = -SdT - M.dB \tag{1.12}$$

This equation shows that the transition from the normal to the superconducting state is coming with a gain in the energy. This is because of the fact that the free energy of a material is higher in the normal state. In the superconducting state, conduction electrons are paired in single quantum states with the lower energy. A superconducting material is affected by the applied magnetic field and the magnetic moment generated antiparallel to that applied magnetic field. By considering $G_s(T, 0)$ the Gibbs function of superconducting state with zero magnetic field, $G_s(T, B)$ the Gibbs function of superconducting state with magnetic field B and $(\frac{\partial G}{\partial B})_T = -M$, we can get to:

$$G_s(T, B) - G_s(T, 0) = \frac{1}{2\mu_0} B^2 \tag{1.13}$$

The difference between the two terms above is equal to the increase in the Gibbs free energy per unit volume. At the transition magnetic field B_c, normal and superconducting states are in equilibrium. By considering $G_n(T, B)$ as G function in the normal state with magnetic field B,

$$G_n(T, B_c) = G_s(T, B_c) \tag{1.14}$$

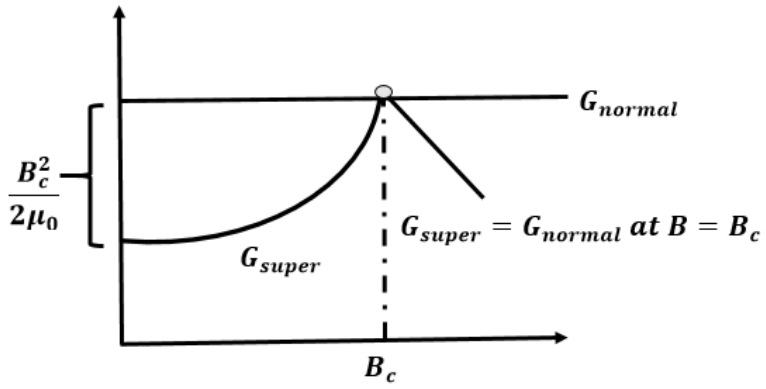

Figure 1.1: Schematic sketch of free energies as a function of magnetic field [36].

By substituting eq.1.14 in eq.1.13, we get to:

$$G_s(T,0) = G_n(T,0) - \frac{1}{2\mu_0}B_c^2 \tag{1.15}$$

which shows for $B > B_c$, the superconductivity is going away. Fig.1.1 is an illustration of what we have discussed above. In order to go from the normal to the superconducting state the material has to push out the magnetic energy, and the largest amount it can push out is the difference between the two free energies at vanishing field.

Ginzburg-Landau theory

In 1950, Ginsburg and Landau introduced a complex order parameter called ψ which is a complex pseudo-wave function. They also introduced $|\psi|^2$ which is proportional to the local density of the superconducting electrons [32]. Ginzburg-Landau (GL) theory is able to explain the macroscopic behavior of the superconductors, specially the type II ones. This theory assumes that the value of ψ is not equal to zero only in the superconducting state [43]. The basic postulation of this theory is that ψ and its gradient are small and vary slowly in the space which makes this theory to be applicable only for temperatures close to T_c [4]. In this theory Gibs free energy has a

very important role. The difference between normal and superconducting Gibbs free energy in the presence of magnetic filed B is shown in terms of $|\psi|^2$ and its gradient $|\nabla\psi|^2$,

$$g = g_n + a|\psi|^2 + \frac{b}{2}|\psi|^4 + \frac{1}{2m^*}|(-i\hbar\nabla - 2eA)\psi|^2 + \frac{|B|^2}{2\mu_0} \tag{1.16}$$

in the above equation, the free energy density of normal state is shown by g_n, quasi-particle effective mass by m^* and magnetic vector potential by A. Here a and b are both phenomenological and temperature dependent parameters. In the case of weak gradients and fields, the above equation will change into:

$$g = g_n + a|\psi|^2 + \frac{b}{2}|\psi|^4 \tag{1.17}$$

The minimum of free energy occurs when derivative of g is zero with respect to ψ. By taking derivative of Eq.1.17:

$$a\psi + b\psi|\psi|^2 = 0 \tag{1.18}$$

By considering the fact that a has a negative constant value, we can find the maximum value of ψ to be:

$$|\psi_m|^2 = -\frac{a}{b} \tag{1.19}$$

here $|\psi_m|^2$ is the density of electrons inside the superconductor, where it is screened from any surface currents and fields. If we put the value of Eq.1.19 back into Eq.1.17 we get to:

$$g - g_n = -\frac{a^2}{2b} = -\frac{|B_c|^2}{2\mu_0}, \tag{1.20}$$

In this equation the maximum value of magnetic field B_c is calculated by considering $B_c^2 = \mu_0 a^2/b$. By using Eq.1.10 we can get to both GL coefficients:

$$\begin{aligned} a &= -\frac{\lambda^2 B_c^2 e^2}{m^* c^2} \\ b &= \frac{16\mu_0\lambda^4 B_c^4 e^4}{m^{*2} c^4} \end{aligned} \tag{1.21}$$

if we also include the presence of gradients and fields, ψ can be written in the form of:

$$\psi(r) = \psi_0 e^{i\varphi(r)} \tag{1.22}$$

ψ_0 here is the amplitude value which is constant. If we substitute $\psi(r)$ into Eq.1.15 and take the derivative of that equation with respect to ψ we get to:

$$a\psi_0 + b\psi_0^3 + \frac{\hbar^2}{2m^*}\psi_0 e^{-i\varphi}(i\nabla + \frac{2\pi}{\Phi_0}A)^2 e^{i\varphi} = 0, \tag{1.23}$$

in above equation the fluxoid quantum is shown by $\Phi_0 = \frac{h}{2e}$. In the cases where the gradient of the phase is small, $\nabla^2\varphi$ is negligible and we can rewrite the equation in the form of:

$$a + b\psi_0^2 + \frac{\hbar^2}{2m^*}(\nabla\varphi - \frac{2\pi}{\Phi_0}A)^2 = 0. \tag{1.24}$$

This equation is called the first GL equation and value of ψ_0 can be derived out of that.

Coherence length and penetration depth

Later on Ginsburg and Landau introduced a new parameter called the coherence length ξ, which is the length scale that indicates the variation of order parameter. If we assume there is perfect Meissner effect, we have $A = 0$ inside the superconductor. If we also consider the fact that $a < 0$, Eq.1.24 will change to:

$$\frac{\hbar^2}{2m^*|a|}(\nabla\varphi)^2 = 1 - \frac{b}{|a|}\psi_0^2. \tag{1.25}$$

for the case of $\psi_0 = |\psi_m|$, the above equation will be equal to zero. The coherence length value defined by Ginzburg and Landau then will be:

$$\xi^2(T) = \frac{\hbar^2}{2m^*|a(T)|} \propto \frac{1}{1-t}, \tag{1.26}$$

where here $t = \dfrac{T}{T_c}$. The temperature dependence of coherence length is phenomenological and the magnitude of $\xi(T)$ can be calculated by taking the square root of

above equation:

$$\xi(T) = \sqrt{\frac{\hbar^2}{2m^*|a(T)|}}, \tag{1.27}$$

In GL theory, the value of current density j is:

$$j = -\frac{i\hbar e}{m^*}(\psi^*\nabla\psi - \psi\nabla\psi^*) - \frac{4e^2}{m^*}A|\psi|^2 \tag{1.28}$$

By substituting Eq.1.22 in above equation we will have:

$$\psi^*\nabla\psi - \psi\nabla\psi^* = 2i\psi_0^2\nabla\varphi \tag{1.29}$$

then the value of current density will be:

$$j = \frac{2\hbar e}{m^*}\psi_0^2(\nabla\varphi - \frac{2\pi}{\Phi_0}A) \tag{1.30}$$

by taking curl of the current density,

$$\nabla \times j = -\frac{4\pi\hbar e\psi_0^2}{m\Phi_0}\nabla \times A = -\frac{4e^2\psi_0^2}{m^*}B \tag{1.31}$$

Ginsburg and Landau were able to find other important parameters. By comparing the above equation with second London's equation (Eq.1.8), they introduced a new parameter called penetration length (λ_{eff}). λ_{eff} is a length scale that indicates how far B penetrates into the material.

$$\lambda_{eff}^2 = \frac{m^*}{4\mu_0 e^2\psi_0^2}. \tag{1.32}$$

London brothers in their theory considered ϕ to be a constant number and by their assumption $\nabla\varphi = 0$. In GL frame, the local density of electrons is $n_s = |\psi|^2$ and if we consider that, this equation agrees with London penetration depth. Then the value of n_s is calculated to be:

$$n_s = \frac{m^*}{4\mu_0 e^2\lambda_{eff}^2}. \tag{1.33}$$

Upper critical field

In the case of very large magnetic fields, $|\psi|^2 \ll |\psi_m|^2 = -a/b$ and only terms with the lowest order of ψ are kept in the GL free energy equation [28]. By taking derivative of Eq.1.16 with respect to ψ we have:

$$(\frac{\nabla}{i} - \frac{2\pi}{\Phi_0}A)^2\psi = -\frac{2m^*a}{\hbar^2}\psi = \frac{\psi}{\xi^2}. \tag{1.34}$$

by assuming a parallel field in z direction and use of Maxwell's equation $B = \nabla \times A$, we get $(A_x, A_y) = (0, Bx)$,

$$[-\nabla^2 + i2\frac{2\pi B}{\Phi_0}x\frac{\partial}{\partial y} + (\frac{2\pi B}{\Phi_0})^2x^2]\psi = \frac{\psi}{\xi^2}. \tag{1.35}$$

Because of the fact that the vector potential is only x dependent, the value of ψ will be:

$$\psi = f(x)e^{ik_y y}e^{ik_z z} \tag{1.36}$$

if we substitute that in Eq.1.35, we get to:

$$-f'' + (\frac{2\pi B}{\Phi_0})^2(x - x_0)^2 f = (\frac{1}{\xi^2} - k_z^2)f \tag{1.37}$$

In the above equation we have $x_0 = k_y\Phi_0/2\pi B$. Eigenfunctions of this equation can be calculated by solving the Schrödinger equation for a particle in a harmonic oscillator potential,

$$f(x) = exp[-\frac{(x - x_0)^2}{2\xi^2}] \tag{1.38}$$

This equation shows the amplitude of ψ is changing in the order of ξ. Eigenvalues for these eigenfactors are:

$$B = \frac{\Phi_0}{2\pi(2n + 1)}(\frac{1}{\xi^2} - k_z^2). \tag{1.39}$$

n here can be $0, 1, ...$ Highest value of B only can achieved when $n = 0$ and $k_z = 0$. This maximum value is called upper critical magnetic field which is a very important parameter in superconductivity are and is equal to:

$$B_{c2} = \frac{\Phi_0}{2\pi\xi^2}. \tag{1.40}$$

Ginsburh and Landau also introduced a very important dimensionless parameter called GL parameter,

$$\kappa = \frac{\lambda}{\xi} \tag{1.41}$$

by considering Eq.1.40, Eq.1.26 and Eq. 1.20, we get to

$$B_{c2} = \sqrt{2}\kappa B_c. \tag{1.42}$$

the value $\kappa = 1/\sqrt{2}$ is classifying superconductors into two different types. If $\kappa < 1/\sqrt{2}$ then $B_c > B_{c2}$ and the superconductor is the type I superconductor. If $\kappa > 1/\sqrt{2}$ then $B_c < B_{c2}$ and the superconductor is a type II one. The temperature dependence of the critical field can often approximated by the expression:

$$B_c(T) = B_c(0)[1 - t^2] \tag{1.43}$$

where, $t = T/T_c$ in the above equation.

BCS theory

In 1957, Bardeen, Cooper, and Schrieffer [5] were able to explain the concept of superconductivity for the temperatures very close to zero Kelvin. This microscopic theory is referred to as the BCS theory by other people in the field. In BCS theory, a new term called energy gap is introduced which is separating the excited state in the superconductor from the ground state. Many properties of the superconductivity can be explained by this theory. In addition, the microscopic base of GL theory can be derived from BCS theory, which makes this theory more valuebale [15]. It was for the firts time in 1950 that Fröhlich [13] pointed out the importance of interaction between electrons and lattice. When an electron is passing by, lattice will be pulled toward that electron. When another electron is passing by with the same momentum but opposite direction, it will be attracted at the same position by the displaced lattice as shown in Fig.1.2. This interaction results in an effective attraction between

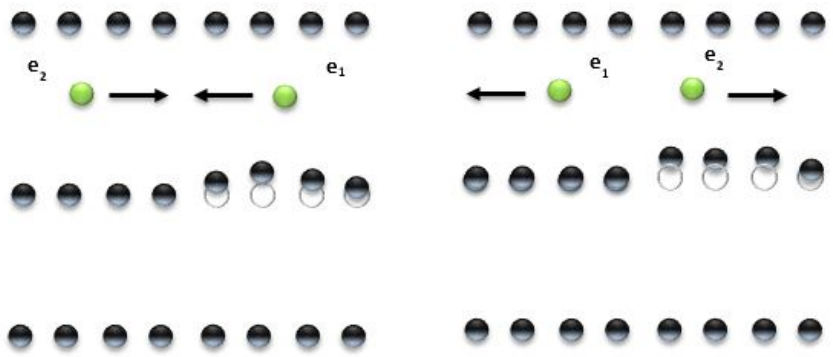

Figure 1.2: A qualitative demonstration of pair attraction phenomena that is mediated by the lattice. The electron 1 induces a distortion in the lattice. When the electron 2 passes by that distortion, its state is being affected.

electrons and a phonon is exchanged between electrons through the lattice. If this attractive force is strong enough to overcome the screened Coulomb repulsive force, a net attractive interaction will be increased and the material becomes superconductor.

In 1951 Reynolds et al. [38], discovered the isotope effect in mercury for the first time, which was able to support the Fröhlich theory. In their experimental results, they observed parabolic relationship of T_c and B_c with isotopic mass M(T_c and $B_c \propto M^{-1/2}$). If electrical conduction in mercury were purely electronic, there should be no dependence upon the nuclear masses. This dependence of the critical temperature for superconductivity upon isotopic mass was the first direct evidence for interaction between the electrons and the lattice. This assumption, supported the BCS theory of lattice coupling of electron pairs. It is quite remarkable that an electrical phenomenon like the transition to the zero resistivity should involve a purely mechanical property of the lattice. Since a change in the critical temperature involves a change in the energy environment associated with the superconducting transition. This suggests that part of the energy is being used to move the atoms of the lattice, since the energy depends upon the mass of the lattice. It also indicates that lattice vibrations are a part of the superconducting process. In 1956, Cooper [10] showed that every two electrons in the Fermi sea, due to the attractive weak

interaction between them can bind and form a bound state called Cooper pair.

Cooper showed that even a weak attraction can bind pairs of electron into a bound state and the Fermi sea of electrons is unstable against the formation of at least one bound pair, regardless of how weak the interaction is, so long as it is attractive. According to this theory, as one electron passes by positively charged ions in the lattice of the superconductor, the lattice distorts and the center of positive charge shifts. Virtual phonons are emitted and form a cloud of positive charges around the electron. After the electron passes, but before the lattice springs back to its normal position, a second electron is drawn to the cloud. It is through this process that two electrons, which should repel one another, get connected. As one electron of a Cooper pair passes close to an ion in the lattice, the attraction between them causes a vibration. This vibration can be passed from ion to ion until the other electron of the Cooper pair absorbs the vibration. The net effect is that the electron has emitted a phonon and the other electron has absorbed the phonon. In a simple model, it is assumed that when a pair of electrons are added to the Fermi level, they only interact with each other. For achieving the lowest energy state, these two electrons should have a total momentum of zero. In order for that to happen, they should have their momentum equal and opposite to each other. The wave function of this pair then will be:

$$\psi_0(\mathbf{r}_1, \mathbf{r}_2) = \sum_{\mathbf{k}} g_{\mathbf{k}} e^{i\mathbf{k}\cdot(\mathbf{r}_1 - \mathbf{r}_2)} \chi(1,2) \tag{1.44}$$

here $\chi(1,2)$ is the spin coupling function and $g_{\mathbf{k}}$ is the weighting coefficient. In general, spin function can be chosen from one of both antisymmetric singlet spin function $(\uparrow\downarrow - \downarrow\uparrow)$ or symmetric triplet spin functions $(\uparrow\uparrow, \uparrow\downarrow + \downarrow\uparrow, \downarrow\downarrow)$. In this case, the singlet one is used because the singlet coupling restricts the orbit function to be a sum over $\cos\mathbf{k}\cdot(\mathbf{r}_1 - \mathbf{r}_2)$ and provides lower energy than the triplet one. $\sum \cos\mathbf{k}\cdot(\mathbf{r}_1 - \mathbf{r}_2)$ term has a larger probability amplitude for the electrons close to

each other than other terms. Wave function then will be:

$$\psi_0(\mathbf{r}_1 - \mathbf{r}_2) = [\sum_{\mathbf{k}>\mathbf{k_F}} g_{\mathbf{k}} \cos \mathbf{k} \cdot (\mathbf{r}_1 - \mathbf{r}_2)](\uparrow\downarrow - \downarrow\uparrow) \tag{1.45}$$

for calculating BCS ground state function, second quantization language is commonly used by physicists. In this language, the occupied states are shown by using creation operator $c^*_{\mathbf{k}\uparrow}$, which is creating an electron with the momentum $\mathbf{k}$ and the spin up. Empty states are shown by the annihilation operator $c_{\mathbf{k}\uparrow}$, to annihilates an electron with the same momentum and spin. By considering these conditions, the ground state wave function will be:

$$|\psi_G\rangle = \Pi_{\mathbf{k}=\mathbf{k}_1,\ldots,\mathbf{k}_M}(u_{\mathbf{k}} + v_{\mathbf{k}} c^*_{\mathbf{k}\uparrow} c^*_{-\mathbf{k}\downarrow})|\psi_0\rangle \tag{1.46}$$

Here the probability of one pair $(\mathbf{k}\uparrow, -\mathbf{k}\downarrow)$ being occupied or unoccupied is shown by $|v_{\mathbf{k}}|^2$ and $|u_{\mathbf{k}}|^2$ respectively and the probability $|u_{\mathbf{k}}|^2$ is equal to $1 - |v_{\mathbf{k}}|^2$. In later calculations, the magnitudes of $u_{\mathbf{k}}$ and $v_{\mathbf{k}}$ are calculated. In the cases where only the attraction between the pair of electrons is considered, the pairing or reduced Hamiltonian is applicable. The Hamiltonian can be written:

$$H = \sum_{\mathbf{k}\sigma} \epsilon_{\mathbf{k}} c^*_{\mathbf{k}\sigma} c_{\mathbf{k}\sigma} + \sum_{\mathbf{kl}} V_{\mathbf{kl}} c^*_{\mathbf{k}\uparrow} c^*_{-\mathbf{k}\downarrow} c_{\mathbf{l}\uparrow} c_{-\mathbf{l}\downarrow} \tag{1.47}$$

$\epsilon_{\mathbf{k}}$ here is representing the kinetic energy of the electrons. In this approach, it is considered that operators like $c_{\mathbf{k}\uparrow} c_{-\mathbf{k}\downarrow}$ can have non zero expectation values, unlike normal state. Fluctuations about the expectation values are very small because of large number of particles. In this approach also it is suggested to use the product of operators in the form of $c_{-\mathbf{k}\downarrow} c_{\mathbf{k}\uparrow} = b_{\mathbf{k}} + (c_{-\mathbf{k}\downarrow} c_{\mathbf{k}\uparrow} - b_{\mathbf{k}})$ in Eq.1.47. The value $b_{\mathbf{k}}$ here is determined self-consistently, so:

$$b_{\mathbf{k}} = < c_{-\mathbf{l}\downarrow} c_{\mathbf{l}\uparrow} >_{av}$$

Now model-Hamiltonian is formed as,

$$H = \sum_{\mathbf{k}\sigma} \epsilon_{\mathbf{k}} c^*_{\mathbf{k}\sigma} c_{\mathbf{k}\sigma} + \sum_{\mathbf{kl}} V_{\mathbf{kl}} (c^*_{\mathbf{k}\uparrow} c^*_{-\mathbf{k}\downarrow} b_{\mathbf{l}} + b^*_{\mathbf{k}} c_{\mathbf{l}\uparrow} c_{-\mathbf{l}\downarrow} - b^*_{\mathbf{k}} b_{\mathbf{l}}) \tag{1.48}$$

the value for energy gap is defined as:

$$\Delta_{\mathbf{k}} = -\sum_{\mathbf{l}} V_{\mathbf{kl}} b_{\mathbf{l}} \tag{1.49}$$

The next step is to do linear transformation in order to diagonalize the above equation. The appropriate transformation can be done by defining new Fermi operators $\phi_{\mathbf{k}}$ and $\phi^*_{\mathbf{k}}$,

$$\begin{aligned} c_{\mathbf{k}\uparrow} &= u^*_{\mathbf{k}}\phi_{\mathbf{k}} + v_{\mathbf{k}}\phi^*_{-\mathbf{k}} \\ c^*_{-\mathbf{k}\downarrow} &= -v^*_{\mathbf{k}}\phi_{\mathbf{k}} + u_{\mathbf{k}}\phi^*_{-\mathbf{k}} \end{aligned} \tag{1.50}$$

by substituting new operators in model Hamiltonian we obtain:

$$\begin{aligned} H = &\sum_{\mathbf{k}} \epsilon_{\mathbf{k}}[(|u_{\mathbf{k}}|^2 - |v_{\mathbf{k}}|^2)(\phi^*_{\mathbf{k}}\phi_{\mathbf{k}} + \phi^*_{-\mathbf{k}}\phi_{-\mathbf{k}}) + 2|v_{\mathbf{k}}|^2 + 2u^*_{\mathbf{k}}v^*_{\mathbf{k}}\phi_{-\mathbf{k}}\phi_{\mathbf{k}} \\ &+ 2u_{\mathbf{k}}v_{\mathbf{k}}\phi^*_{\mathbf{k}}\phi^*_{-\mathbf{k}}] + \sum_{\mathbf{k}}[(\Delta_{\mathbf{k}}u_{\mathbf{k}}v^*_{\mathbf{k}} + \Delta^*_{\mathbf{k}}u^*_{\mathbf{k}}v_{\mathbf{k}})(\phi^*_{\mathbf{k}}\phi_{\mathbf{k}} + \phi^*_{-\mathbf{k}}\phi_{-\mathbf{k}} - 1) \\ &+ (\Delta_{\mathbf{k}}v^{*2}_{\mathbf{k}} - \Delta^*_{\mathbf{k}}u^{*2}_{\mathbf{k}})\phi_{-\mathbf{k}}\phi_{\mathbf{k}} + (\Delta^*_{\mathbf{k}}v^2_{\mathbf{k}} - \Delta_{\mathbf{k}}u^2_{\mathbf{k}})\phi^*_{\mathbf{k}}\phi^*_{-\mathbf{k}} + \Delta_{\mathbf{k}}b^*_{\mathbf{k}}] \end{aligned} \tag{1.51}$$

$\phi_{\mathbf{k}}$ is like $c_{\mathbf{k}\uparrow}$ and can destroy an electron with $\mathbf{k}\uparrow$ or create one with $-\mathbf{k}\downarrow$. Next step is to choose $u_{\mathbf{k}}$ and $v_{\mathbf{k}}$ as shown below, in order to eliminate crossing terms $\phi_{\mathbf{k}}\phi_{-\mathbf{k}}$ and $\phi^*_{\mathbf{k}}\phi^*_{-\mathbf{k}}$,

$$2\epsilon_{\mathbf{k}}u_{\mathbf{k}}v_{\mathbf{k}} + \Delta^*_{\mathbf{k}}v^2_{\mathbf{k}} - \Delta_{\mathbf{k}}u^2_{\mathbf{k}} = 0 \tag{1.52}$$

by multiplying above equation by $\dfrac{\Delta^*}{u^2_{\mathbf{k}}}$, we get to a quadratic equation. The solution to this equation is:

$$\frac{\Delta^*_{\mathbf{k}}v_{\mathbf{k}}}{u_{\mathbf{k}}} = \sqrt{\epsilon^2_{\mathbf{k}} + |\Delta_{\mathbf{k}}|^2} - \epsilon_{\mathbf{k}} \tag{1.53}$$

the next step is to introduce $E_{\mathbf{k}}$ as excitation energy of a fermion which is positive and greater than Δ,

$$E_{\mathbf{k}} = \sqrt{\epsilon^2_{\mathbf{k}} + |\Delta_{\mathbf{k}}|^2} \tag{1.54}$$

by considering normalization requirement $|u_{\mathbf{k}}|^2 + |v_{\mathbf{k}}|^2 = 1$, exact values of $u_{\mathbf{k}}$ and $v_{\mathbf{k}}$ coefficients can be calculated as below,

$$\begin{aligned} |u_{\mathbf{k}}|^2 &= \frac{1}{2}(1 + \frac{\epsilon_{\mathbf{k}}}{E_{\mathbf{k}}}) \\ |v_{\mathbf{k}}|^2 &= \frac{1}{2}(1 - \frac{\epsilon_{\mathbf{k}}}{E_{\mathbf{k}}}) \end{aligned} \tag{1.55}$$

by the use of Eq.1.50 in Eq, 1.49, $\Delta_{\mathbf{k}}$ can be written in the form of:

$$\Delta_{\mathbf{k}} = -\sum_{\mathbf{l}} V_{\mathbf{kl}} u_{\mathbf{l}}^* v_{\mathbf{l}} \langle 1 - \phi_{\mathbf{k}}^* \phi_{\mathbf{k}} - \phi_{-\mathbf{k}}^* \phi_{-\mathbf{k}} \rangle \tag{1.56}$$

here $\phi_{\mathbf{k}}^* \phi_{\mathbf{k}}$ and $\phi_{-\mathbf{k}}^* \phi_{-\mathbf{k}}$ are number operators of excited Fermi quasi-particles. The probability of excitation in normal state equation is in the form of Fermi function:

$$f(E_{\mathbf{k}}) = \frac{1}{e^{\beta E_{\mathbf{k}}} + 1} \tag{1.57}$$

in above equation $\beta = 1/kT$. By considering $E_{\mathbf{k}}$ to be a positive number at $T = 0$ Fermi function goes to zero. The BCS energy gap can be written in the form of:

$$\Delta_{\mathbf{k}} = -\sum_{\mathbf{l}} V_{\mathbf{kl}} u_{\mathbf{l}}^* v_{\mathbf{l}} [1 - 2f(E_{\mathbf{l}})] = -\sum_{\mathbf{l}} V_{\mathbf{kl}} \Delta_{\mathbf{l}} \frac{\tanh \beta E_{\mathbf{l}}/2}{2E_{\mathbf{l}}} \tag{1.58}$$

Cooper considered the approximation of $V_{\mathbf{kk'}} = -V$ and by assuming that, was able to calculate the energy gap for isotropic (s-wave) superconductors. He also assumed that the energy gap of the s-wave superconductor is independent of the momentum k. By considering all of these assumptions, the above equation will be:

$$\frac{1}{V} = \sum_{\mathbf{k}} \frac{\tanh \beta E_{\mathbf{k}}/2}{2E_{\mathbf{k}}} \tag{1.59}$$

by the use of Eq. 1.54 and changing the sum to the integral, we get to:

$$\frac{1}{N(0)V} = \int_0^{\hbar\omega_c} \frac{1}{\sqrt{\epsilon_k^2 + \Delta^2(0)}} d\epsilon = \int_0^{\hbar\omega_c/\Delta(0)} \frac{1}{\sqrt{1+x^2}} dx. \tag{1.60}$$

here $N(0)$ is the density of the electrons at the Fermi surface. At temperature T_c, the value of $\Delta(T)$ goes to zero. In that point, the excitation spectrum is equal to the normal state one and we have $\epsilon_k = E_{\mathbf{k}}$. By replacing $E_{\mathbf{k}}$ to ϵ_k, we can solve the above equation numerically. By taking the symmetry of ϵ_k above Fermi level into the calculations, we get to:

$$\frac{1}{N(0)V} = \int_0^{\beta_c \hbar\omega_c/2} \frac{\tanh x}{x} dx = \ln 2e^{\gamma} \beta_c \hbar\omega_c/\pi \tag{1.61}$$

γ is the Euler's constant and is equal to 0.577.... Now kT_c can be defined as:

$$kT_c = 1.13 \hbar\omega_c e^{-1/N(0)V}. \tag{1.62}$$

In the case of weak coupling limits, we have $N(0)V \ll 1$. By substituting Eq.1.62 in Eq.1.60 we get to the value of gap at zero Kelvin:

$$\Delta(0) = \frac{\hbar\omega_c}{\sinh(1/N(0)V)} \approx 2\hbar\omega_c e^{-1/N(0)V} = 1.764kT_c, \tag{1.63}$$

Above equation shows that the value of the gap at $T = 0$ is comparable in the energy with kT_c value. At the temperature T, the following approximation solution is applicable:

$$\frac{\Delta(t)}{\Delta(0)} \approx 1.74\sqrt{1-t} \tag{1.64}$$

where, $t = T/T_c$.

Chapter 2

Transport behavior of superconductors

In 1952, Abrikosov introduced the type II superconductors for the fist time [2]. These types of superconductors, for the applied magnetic fields between the lower magnetic field B_{c1} and the upper mgnetic field B_{c2}, enter the mixed state. Mixed state contains magnetic flux vortices carrying a total flux equal to $\Phi_0 = \frac{h}{2e}$. Each vortex is like one elementary cell, which supercurrent is circulating around one normal core. By increasing the magnetic field, the supeconducting gap Δ starts to shrink in the core of the vortex and the core itself becomes surronded by the circulating supercurrents. Abrikosov vortices in type II superconductors not only can be generated by applying magnetic filed, but also because of the thermal fluctuations spontaneously [27].

Transport behavior in the superconductors have three different regimes as a function of current density j. Below j_c, system shows perfect conductivity. But it is dissipative between j_c and j_d and normal above j_d as it is shown in Fig.2.1. In the mixed state, the transport current interacts with the vortices and exerts a driving

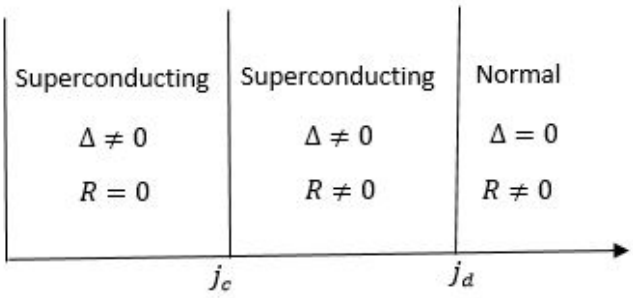

Figure 2.1: Three different regimes in order to compare the transport behavior of a superconductor [31]

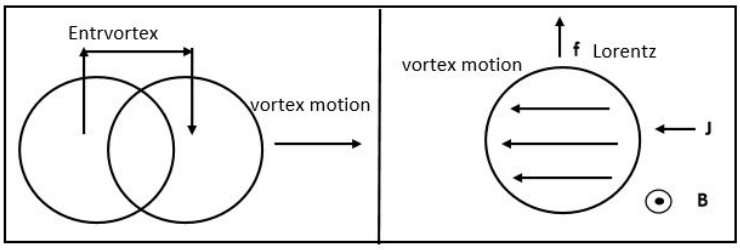

Figure 2.2: Energy dissipation during the motion of vortex [21]

Lorentz force on them. Motion of vortices lead to the dissipation, a finite electric filed E and appearance of resistivity ρ. The motion of a single vortex in a type II superconductor is demonstrated in Fig. 2.2. The vortex while moving, transfers the entropy from the trail end to the lead face (left panel of Fig.3). In a different approach by Bardeen and Stephen [6], the electric field in the core that is generated by magnetic field and is changing with respect to the time, can be calculated by the use of Maxwell equation in the middle of the normal core. Bardeen and Stephen used London equations to describe the superconductivity, outside the core (right panel of Fig.3).

Several interactions can affect the flux motion, which can result in different regimes in the I-V characteristic measurements. In the case of low driving forces and high temperatures, the motion of vortices is mainly due to thermally-activated depinning and there will be very weak current dependence resistivity. In this regime behavior is ohmic and it is called thermally activated free flux regime ($TAFF$). By increasing j, current-drivven depinning starts competing with the thermal activation in a non-linear regime. By increasing of j, flux motion enters the new regime called free flux flow (FFF), which is an idealized case of vortex moving without pinning. This regime is ohmic and the equation of motion is dominated by the Lorentz force and the drag viscous. As current increases, it starts to suppress the superconducting energy gap to the point where the kinetic energy overcomes the condensation energy. This regime

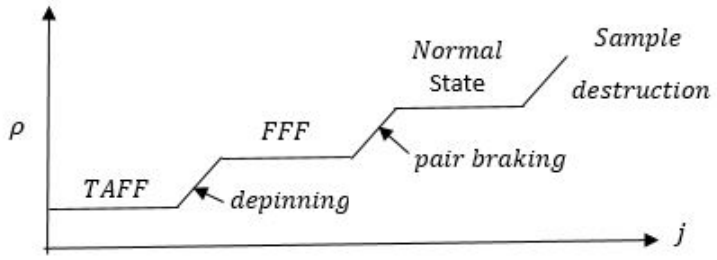

Figure 2.3: Ohmic and non-Ohmic trasport as a function of j [21]

is called pair breaking regime, which is non-ohmic and the resitivity of material goes back to normal. All these regimes are demonstrated in Fig.2.3.

Flux motion

The motion of flux in the mixed state, increases the dissipation inside the superconducting material [21]. A finite value for j_c is needed because of the pinning of the vortices by the defects. How the immobilized vortices are moving is an important topic in studying the current in type II superconductors and it is at the same time controversial. j_{c0} is the value of current in which the Lorentz driving force ($F_L = J \times B$) that is exerted by the current is equal to the pinning force (F_p). In the case of motion of isolated vortices, $f_p = f_l = j_{c0} \times \Phi_0$ is giving the depinning threshold (lower case symbols are quantities per length). Because of the fact that thermal fluctuation is aiding depinning, the effective critical current j_c is less than j_{c0}. By increasing the current, depining starts, but the motion of vortices are damped because of the viscous drag $f_d = \eta v$. For the driving forces more than the depinning threshold, the motion of vortices is called Flux Flow. The Free Flux Flow (FFF) term is describing an ideal case of vortices being isolated and moving without pinning. In FFF regime there is a balance between the driving force and the viscous drag, so that $f_L = j \times \Phi_0 = f_d = \eta v$ and for a constant η value, electric field is proportional to the

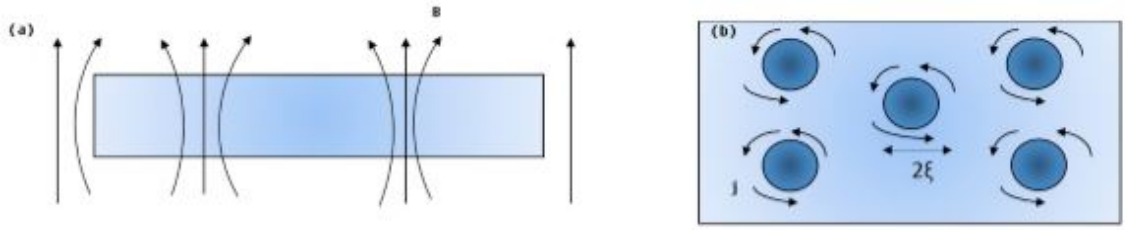

Figure 2.4: (a) Side view of the vortices: Here solid lines represent the B lines (b) Top view: The current directions are shown, here 2ξ is the estimated size of one vortex.

applied current ($E = v \times B/c$ and $\rho = B\Phi_0/\eta c$). Different approaches have been used for calculating η and ρ in details by different authors. But, they are similar in a gross level and are summarized as:

1. Vortex core is approximated by a normal cylinder with radius ξ (coherence length)

2. Vortex motion is generating an electric field inside the core which results into normal current density and is roughly equal to suppercurrent density outside.

Side view and top view of vortices is shown in Fig. 2.4.

For a particle with mass m in a viscous medium, it takes a long time to get to its final drift velocity. For a vortex because of negligible mass, it accelerates to its final velocity almost instantaneously. In all the equations in superconductivity, this average drift velocity is used.

Vortex Viscosity

Vortices appear transparent to the current that is flowing right into them, because of the fact that their motion is generating electric field inside them [39]. In this case the average of macroscopic resistivity will be equal to the normal-state resistivity which is the resistivity inside the core multiplied by the fractional volume that is occupied by the vortices. The resulting dissipation is well explained by Bardeen-Stephen equation

which is a good starting point in the limit of large currents and electric fields.

$$\frac{\rho_{fff}}{\rho_n} \approx \frac{B}{H_{c2}(T)} \tag{2.1}$$

In this region behavior is ohmic, but as the current is increasing, the dissipation will be nonlinear and eventually reaches an instability point which is due to a discontinuous increase in the voltage.

In 1986 Larkin and Ovchinnikov [25] showed that for low temperature limits in a dirty superconductors the Free Flux resistivity is proportional to the value of normal resistivity:

$$\frac{\rho_{fff}}{\rho_n} \simeq 0.9\frac{B}{H_{c2}(T)} \tag{2.2}$$

Almost the same result (without the prefactor 0.9), is obtaining by the Ohmic dissipation in the core and also temporal changes in the value of order parameter. The equation above is calld LO equation and is the equivalent of $\eta \approx \frac{B}{H_{c2}(T)}$.

The instability at the temperatures not very below the critical temperature, has been studied by Larkin and Ovchinnikov. They were able to show that the electron distribution is departing from a thermal distribution when the vortex velocities are high, which causes the change in the superconducting order parameter and also is altering the drag force on the vortices. Their prediction was observing nonlinearity in the current-voltage characteristics and also an instability in the motion of the vortex at the time the vortex reaches a critical velocity v^*. This instability is because of a decrease in the drag force, which happens when the vortex velocity is increasing and is accompanied by a decrease in the size of vortex itself. They also showed that the critical velocity does not depend on the magnetic field [19]. However, there were experiments performed at the lower temperatures on other superconducting materials, also showing a nonlinearity and instability with a totally different dependence of the value of v^* to the magnetic field B. The analysis showed that this new behavior can be explained by a simple model in which the electron gas has a thermal-like

distribution function which is characterized by a temperature that is higher than the lattice and the bath. Larkin and Ovchinnikov suggested this possibility in their paper, without exploring the consequences. When the electron temperature is increasing, the resulting resistivity increases and causes a decrease in the current. This model yields a critical vortex velocity (v^*) at the instability which is proportional to the inverse of magnetic field ($1/B$) [22].

There are a few fundamental physical phenomena that are unfold in the mixed state of superconductor, when the superconductor is subject to very big current and power dissipation levels [29]. There is a sufficiently large current that can destroy the superconducting state (pair-breaking effect) and will be discussed in next chapter. At intermediate current densities (below the onset of pair-breaking) observation of the free viscous flow of flux vortices is expected. In our work we have used a pulsed-current technique to explore this dissipative regime to verify the pair-breaking effect.

Chapter 3

Depairing Current Density in Superconductors

The depairing current density or pair-breaking current is one of the intrinsic parameters that sets a fundamental limit to the survival of superconductivity [24]. This is the current density at which the kinetic energy of the superconducting carriers becomes equal to the binding energy of the Cooper pairs. By increasing T, B and j, the superconducting gap Δ decreases. The boundary at T, B and j phase in which Δ vanishes, separates the superconducting state from the normal state and that is where all these parameters attain their critical values T_c, B_{c2} and j_d respectively. Any of these functions can be separately defined as the critical boundary.

T_c and B_{c2} measurements are done routinely while j_d is seldomly measured, due to the technical difficulties associated with sample heating at the high currents [21]. A series of useful reviews have been given on the calculation of the depairing current densities [26] [23]. These theoretical calculations cover different regimes. The simple London equations are valid at T_c, but it fails at the lower temperatures since it does not take into account the effect of the change in the order parameter with the current. The GL theory gives a good phenomenological treatment that works well close to T_c. For low temperatures, some other theories based on the microscopic theories have been proposed.

Depairing current density in London equations framework

The value of j_d can be obtained in a simple London approach by equating the kinetic energy and condensation energy density expressions,

$$\frac{1}{2}n_s m^* v_s^2 = \frac{B_c^2}{2\mu_0}. \tag{3.1}$$

The current density and velocity in the superconductors are related by:

$$j_s = 2en_s v_s \tag{3.2}$$

by using the value of $v_s = j_s/2en_s$ and Eq.1.5, we have:

$$j_d = \frac{B_c}{\mu_0 \lambda_L} \tag{3.3}$$

In this derivation, it is assumed that n_s is not affected by j when it gets closer to j_d. This formula seems to be far from reality, because it does not consider the fact that density of electrons is changing. But it can give us an idea about the fact that j_d depends on both critical field and the penetration depth.

Depairing current density in Ginzburg-Landau theory framework

Velocity of the quasiparticles in a superconductor can be obtained by equating Eq.1.30 and Eq.3.1,

$$\mathbf{v}_s = \frac{\hbar}{m^*}(\nabla\varphi - \frac{2\pi}{\Phi_0}A). \tag{3.4}$$

If we substitute above equation in (Eq.1.16) and put the derivative of that equal to zero, we can find maximum value for v_s and J_s in which beyond that there wont be any ψ that minimizes the free energy.

$$a + b\psi_0^2 + \frac{1}{2}m^* v_s^2 = 0. \tag{3.5}$$

The optimum of ψ_0 that minimizes free energy at fixed v_s is:

$$\psi_0^2 = \frac{|a|}{b}(1 - \frac{m^* v_s^2}{2|a|}) = |\psi_m|^2[1 - (\frac{\xi m^* v_s}{\hbar})^2]. \tag{3.6}$$

By putting above equation into Eq.3.1, we get to the corresponding supercurrent density:

$$j = 2e|\psi_m|^2[1 - (\frac{\xi m^* v_s}{\hbar})^2]v_s. \tag{3.7}$$

For calculating the maximum current, we put $\frac{\partial j}{\partial v_s} = 0$ and we get to $v_s = \hbar/\sqrt{3}m^*\xi$. This current now can be identified as maximum possible value for the current which is the depairing current value:

$$j_d = \frac{4e|\psi_m|^2\hbar}{3\sqrt{3}m^*\xi}. \tag{3.8}$$

If we combine above equation with London penetration depth equation (Eq.1.5), we eventually get to:

$$j_d = \frac{\hbar}{3\sqrt{3}\mu_0 e\lambda_L^2\xi} = \frac{\Phi_0}{3\sqrt{3}\pi\mu_0\lambda_L^2(T)\xi(T)}. \tag{3.9}$$

by considering $t = T/T_c$, $\lambda_L(t) = \lambda_L(0)/\sqrt{1-(t)^4}$ and $\xi(t) = \xi(0)/\sqrt{1-t}$ for temperatures close to T_c, the shift in T_c at given B and j as a function of applied current can be calculated as:

$$1 - \frac{T_c(j)}{T_c(0)} \approx \left(\frac{1}{4}\right)^{\frac{2}{3}} \left[\frac{j}{j_d(0)}\right]^{\frac{2}{3}} \tag{3.10}$$

In above equation we can see the proportionality of the shift in T_c to $j^{2/3}$. $j_d(0)$ based on above equation will be:

$$j_d(0) = \sqrt{\frac{2\Phi_0}{27\pi\mu_0^2}} \left(\frac{\sqrt{B_{c2}(0)}}{\lambda_L^2(0)}\right), \tag{3.11}$$

here $B_{c2}(0) = \Phi_0/2\pi\xi(0)^2$ is upper critical field at zero temperature. In $MKSA$ system, above equation becomes:

$$j_d(0) = 5.56 \times 10^{-3} \times \sqrt{B_{c2}(0)}/\lambda^2(0), \tag{3.12}$$

here j_d is in A/m^2, B_{c2} is in Tesla and λ is in meters. In above equation, we took off the subscript of λ_L only to prevent confusion. Joule heating can give an apparent

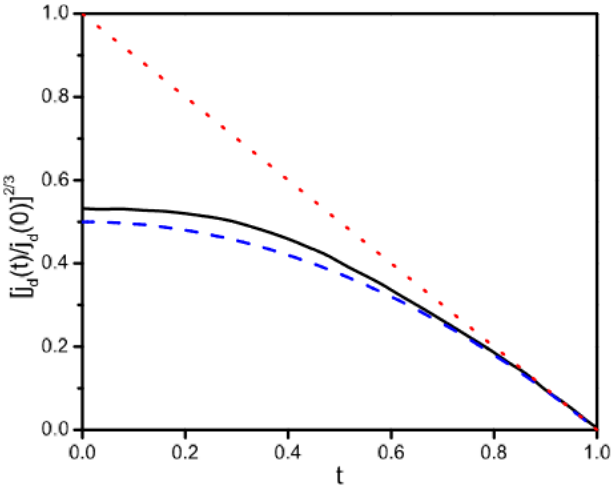

Figure 3.1: Temperature dependence of j_d from different theories. Replotted from Ref.[31]. The solid curve is KL theory, the dashed one is Eq.3.13 and the dot one is GL's result.

shift to T_c ($\Delta T_c \propto \rho j^2$), if for any reason heat removal from the sample is ineffective. Therefore, in any type of measurements, we need to make sure we do not have excessive amount of heating.

Different groups have done calculations for calculating pair breaking current values. Kuprianov and Lukichev [31] among them had closer results to phenomenological expression. They calculated the microscopic j_d value, by inserting temperature dependence of B_c and λ:

$$j_d = \frac{j_d(0)}{2\sqrt{2}}(1-t^2)^{3/2}, \tag{3.13}$$

It is important to point out that the predictions on the temperature dependence of j_d from these theories are the same when the temperature is near T_c.

In order to describe the macroscopic properties such as $j(d)$, the GL theory is more amenable than the BCS microscopic theory [43]. In our lab, both values of $j(d)$ and $B_{c2}(0)$ can be obtained from our transport measurements and is a convenient way to calculate the values of λ and n_s. In addition, unlike some other methods for measuring λ that are unable to provide an accurate absolute value and only are able to provide

$\lambda(T)/\lambda(0)$ (temperature variation), $j(d)$ is able to provide the absolute values for λ and n_s.

Depairing current density from the quasiparticle energy shift

At low temperature limits, in the presence of a uniform velocity v_s the quasiparticle energies shift by $\hbar k_F v_s$ where k_F is the wavevector at the Fermi surface. In superconducting state, n_s stays roughly constant to the point v_s is reaching its critical value v_d. At that point the shift in energy, will be equal to the energy gap and the velocity gets to $v_d = 2\hbar/m^*\xi$ which is the maximum velocity of quasiparticles in GL's framework [20]:

$$v_d = \frac{\Delta}{\hbar k_F} = \frac{2\hbar}{m^*\xi}, \tag{3.14}$$

Here m is the mass of the electron and ξ is the coherence length. j is proportional to v_s until it gets to v_d, where value of n_s is dropping. For the limits where $v_s \ll v_\Delta$, all electrons contribute to supercurrent $j_s = 2en_s v_s$. For temperatures close to T_c, the density of quasi particles is proportional to the order parameter $|\psi|^2$ in GL frame. At low temperatures a more microscopic calculation is required to take into account the effect of the modification on the quasiparticle density by the drifting velocity.

The maximum value that current can get is slightly higher than the value of v_d. By a good approximation it can be said that $j_d \simeq e^* n_s^* v_d$ and:

$$j_d \simeq \frac{m^* c^2 \Delta}{4\pi e^* \lambda^2 \hbar k_F} \simeq \frac{c^2 \hbar}{2\pi^2 e^* \lambda^2 \xi}, \tag{3.15}$$

magnitude of ξ can be calculated by having the information on the value of B_{c2}. Here k_F is a constant number and Δ has temperature dependence. From the right hand side of the above equation the temperature dependence of j_d is calculated in the form of:

$$j_d(T) = j_d(0)(\frac{\lambda^2(0)}{\Delta(0)})\frac{\Delta(T)}{\lambda^2(T)} \tag{3.16}$$

By using the right hand side of Eq.3.15 magnitude of $j_d(0)$ in BCS frame and in $MKSA$ system is estimated to be:

$$j_d(0) = 9.19 \times 10^{-3} \times \sqrt{B_{c2}(0)}/\lambda^2(0), \tag{3.17}$$

which is close to the value of j_d calculated by GL' framework.

Chapter 4

Apparatus and Experimental Techniques

In this chapter the experimental techniques that we have used along the way is discussed.

Sample preparation

Our sample was provided in the form of bulk from $STAR$ Cryoelectronics company in Santa Fe. However, cutting, patterning, etching and wiring was done in our laboratory. They have used DC magnetron sputtering method for sample fabrication. The target that was used in their sputtering machine was $NbTi$ by portions of 70 % Nb and 30 % Ti. The atmosphere was combination of argon and nitrogen gas with the use of silicon as a substrate.

In all our measurements, we have used a four-probe bridge pattern. In order to create this pattern, we first need to make a mask. There are different methods to

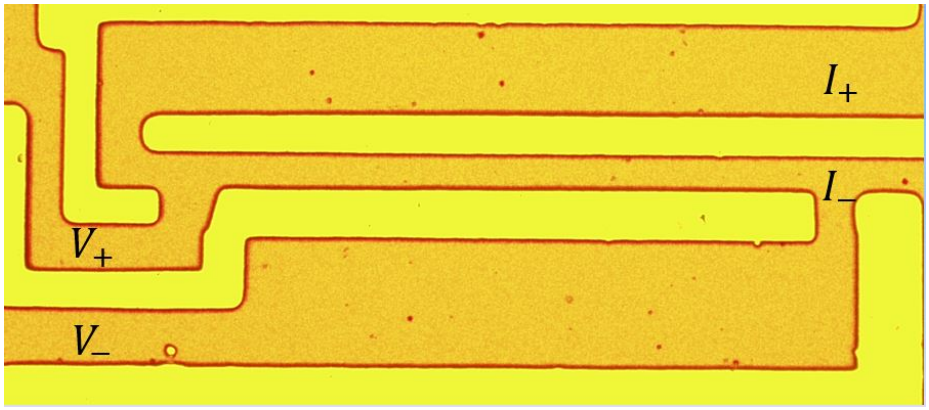

Figure 4.1: Single bridge pattern used in our experiment

make a mask, but we have used the photo lithography method. In this method a camera and projector is needed. The first thing to do was covering a microscope slide with the negative photo resist in the spinner. The next step was to put that slide in the light path of the microscope and exposing the slide to the light for specific amount of time (the time can be different depends on the size of bridge and type of photo resist we use). Then we had to put the slide in the developer which is diluted by water for specific amount of time (depending the exposure time and type of photo resist we have used). All our steps were done in the dark room as there should not be any lighting in the room. After development, by using our sputtering machine, layers of silver was deposited on the slide. The positive pattern remains on the slide and the rest comes off after washing it by acetone. By the use of this mask, the standard photo lithography procedure and ion milling we were able to create the four probe bridge pattern on all of our superconducting film. The length of the bridge that we have created is 200 μm with the width of 11 μm. The aspect ratio (length to the width portion) of the bridge then will be 18.8. After patterning our samples, thin wires were bonded on the micro bridge by indium in order to not have high contact resistance. Then the sample was mounted inside our Cryocooler.

Spin processor

For the photoresist coating purpose, spin coater $WS-650SZ-6NPP/LITE$ from Laurell technologies corporation have been used (Fig.4.2). This compact spinner has some advanced features like automatic control and high-performance and can drive up to 12,000 RPM(rotations per minute). It also comes with multi optional chucks and other advance properties. This system uses high pressure and dry air and for that purpose a compressor is attached to our spin coater machine. The instruction for using this machine is discussed in Appendix A.

Figure 4.2: Spin coater $WS-650SZ-6NPP/LITE$

Sputtering

We have used $PELCO$ model3 sputter coater 91000 (Fig.4.3) in order to do the sputtering process. This sputter coater is an economical desktop unit and is simple to operate. We have used this machine in our laboratory, whenever we wanted to make our own mask or make changes to the masks that we already have. When the pattern is created by the use of photo resist on the slide, a thick layer of metal film should be deposited on the slide. Because of the fact this coater is compact size, pump down time is very fast. In this machine, silver is used as the target. Sputtering is a process whereby particles are ejected from a solid target material due to bombardment of the target by energetic particles, particularly gas ions in a laboratory. Fig.4.4 is a schematic drawing of sputter deposition method. The current controller allows different choices of both sputtering current and argon pressure. Around 20 rounds of deposition is necessary to make a uniform film that we need (to create films in range of μ m). Each round should not take more than 90 seconds in order to prevent the sample being heated up and there should be at least 30 s of wait time between each round. The steps for using the sputtering machine is discussed in Appendix B.

Figure 4.3: $PELCO$ model3 sputter coater 91000

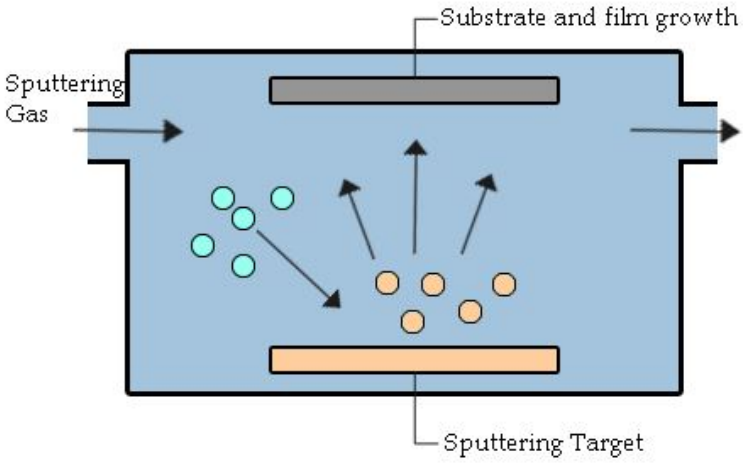

Figure 4.4: Schematic drawing of sputter deposition

Ion-milling system

In order to etch the desired patterns on our superconducting film, we have used an ion milling machine. Ion milling is an etching process, where ions of an inert gas, accelerate from an ion source into the surface of substrate and etch unprotected part (Fig.4.5). In our lab we have two ion-milling systems, Oxford $IG5$ and $TFSIBMS-100$. They are connected together and share the same vacuum system. In our experiments, we only have used the small Oxford $IG5$ which uses a nozzle as

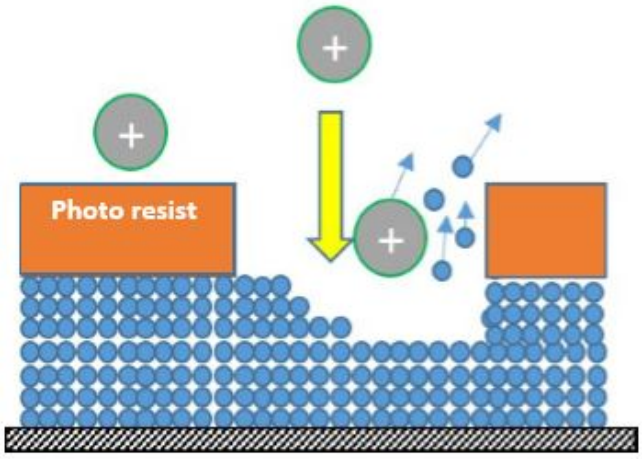

Figure 4.5: Schematic drawing of ion milling process

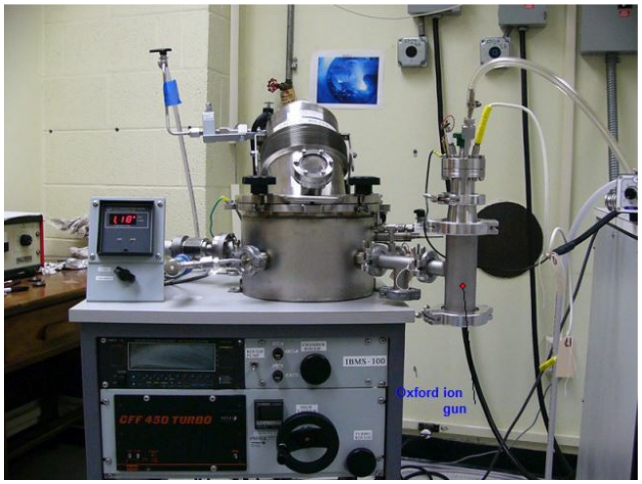

Figure 4.6: Oxford ion gun and $IBMS-100$

an anode (Fig.4.6). The operation of our ion gun machine is discussed in Appendix C.

Cryostats and Magnet

For the transport measurements that we have done in our laboratory for various superconducting samples, $PT405$ cryorefrigerator was used. The standard four-probe measurement wires of the bridge is set up on that. $PT405$ can cool down to the

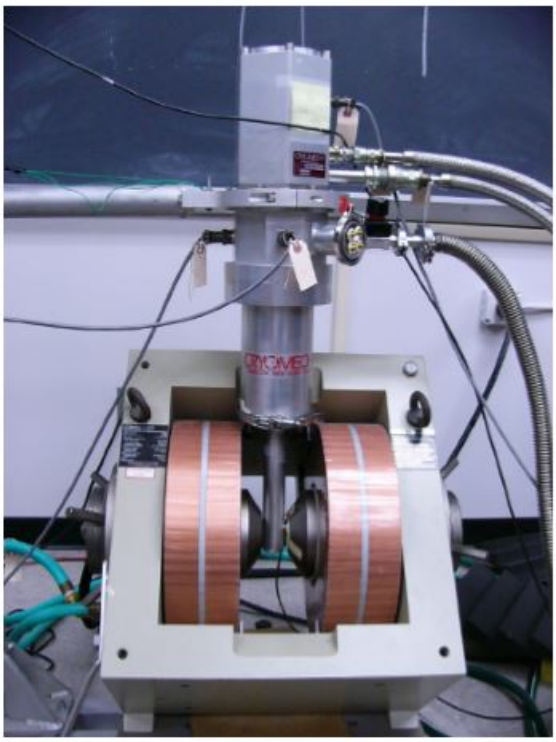

Figure 4.7: $PT405$ Cryostat with $GMW3473$-50 magnet

temperatures lower than 4 K. Most of the samples that we have used, have low T_c and this system perfectly works to reach the temperatures lower than that. $GMW3473$-50 electromagnet installed with our Cryostat Fig.4.7 in order to measure the value of B_c for our samples. The schematic diagram for $PT405$ and $GMW3473$-50 is shown in Fig.4.8.

PT405 refrigerator

$PT405$ is a two stage pulse-tube, closed cycle cryocooler. A Cryomech $CP950$ compressor with frequency of ~ 1.4 Hz is connected to the cooler which requires water to cool down. Before starting the cooling down process, the system was evacuated to $10^{-}5$ *torr* using a turbo-pumping station. When it starts to run, the helium gas is compressing by the compressor and then expanding in the cold head. In this process, the expanded gas is then cooled down and the temperature goes lower.

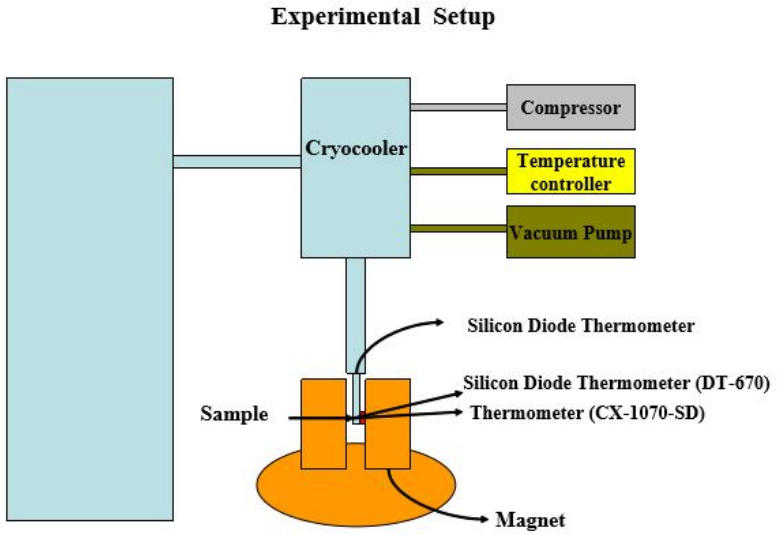

Figure 4.8: Schematic of PT405 and its magnet and sensors

For temperature measurements in this system, three sensors were used:

1. A LakeShore Cernox $CX-1070-SD$ resistance that measures the temperature at the sample position. Temperature can be found by measuring the resistance and use of some time dependent functions. Cernox is the most reliable sensor, because it is stable under the change of both magnetic field and temperature.

2. A LakeShore Diode $DT-670$ which also measures the temperature at the sample position. It indicates the temperature by measuring its cross voltage of the sample. This sensor is used to give a secondary check of the temperature. However this diode is sensitive to temperature and magnetic field.

3. A silicon diode thermometer that measures the temperature at the cold head which is almost 21 cm away from the sample. The reason that this sensor is used is that it is outside where magnetic field is and can give us the feedback of temperature controller.

Schematic drawing of system is shown in Fig.4.8

GMW 3473-50 magnet

Our magnet is water-cooled $GMW\ 3473-50$ with poles of 150 mm made of ferromagnetic iron cores which is used to generate magnetic field at the the point where sample is. this magnet was installed on a rotor and can be rotated horizontally. The maximum current in this magnet is 50 A that can produce a magnetic field of about 1.3 T. To measure the magnetic field, $HGT2100$ Hall probe was used. This sensor is located on one of the iron pole faces. A fixed low current is sent to that probe and the transverse voltage and the produced magnetic field is measured by the use of a multimeter. From the voltage, the transverse resistance can be measured and from the resistance, the magnetic field can be calculated. The reason for that is the fact that the transverse resistance is proportional to the magnetic field. Magnetic field is very stable during all measurements that we do in our lab. The sample holder is located on the end of a copper rod extended from the cold head. The applied magnetic field can be adjusted as the holder is in between the magnet poles.

The Hall effect is the production of a voltage difference (the Hall voltage) across an electrical conductor, transverse to an electric current in the conductor and a magnetic field perpendicular to the current.

DC measurement setup

In order to do our DC measurements, a DC power supply is used in series with a large resistance called ballistic resistance (R_1). The voltage in this power supply can be changed and this power supply is able to provide a continuous low current to the sample (Fig.4.9). One standard resistance is also used in the circuit which is called standard resistance(R_{std}). A Double Pole Double Throw ($DPDT$) relay is used to reverse the current direction in the circuit. By using 4-probe measurement, we can exclude the thermal emf and the contact resistance. By measuring the forward (+) and reversed (−) voltages of the sample and the use of standard resistor, the resistance

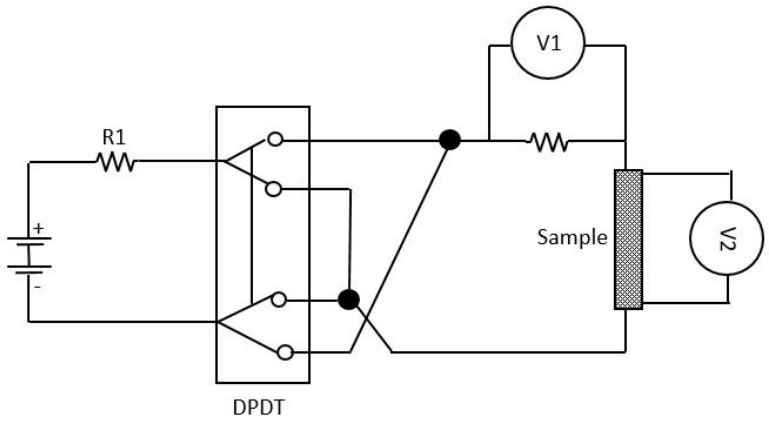

Figure 4.9: DC 4-probe measurement circuit. Computer controls this Double Pole Double Throw ($DPDT$) relay.

of the sample can be calculated:

$$R = R_{std}\frac{\overline{V}^{+}_{sample} - \overline{V}^{-}_{sample}}{\overline{V}^{+}_{std} - \overline{V}^{-}_{std}}, \tag{4.1}$$

All the voltages here are the averages of the readings from our digital multimeters (DMM).

Pulsed measurement setup

For measuring deparing current density in superconductors, high current densities are required. Measurements involving high current densities cause both self heating effect and heat generation from the contacts. Those two can destroy the sample and be a major technical problem. To overcome these problems short-duration, low-duty pulsed current is used rather than continuous DC current. In this approach thermal emf will be subtracted by the oscilloscope itself and there is no need to reverse the direction of the current. Duty cycles can be used to describe the percent time of an active signal in an electrical device such as the power switch in a switching power supply.

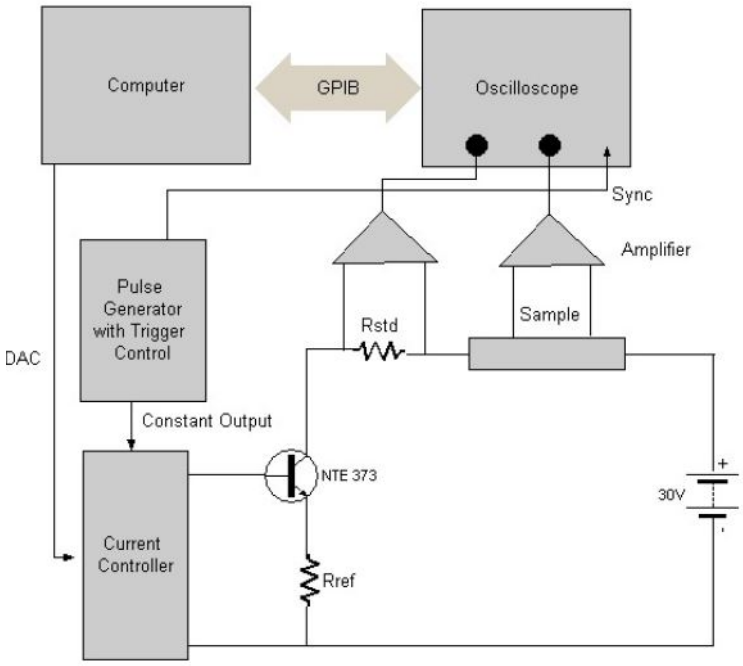

Figure 4.10: Puled measurement setup

The pulse generator which can be both a Wavetek Model 801 or Quantum Composer Model 9512, provides a single-shot pulse with constant amplitude. The pulse is regulated by a current control device and then is feeding the current source which is composed by fast response transistor $NTE373$ and a reference resistor as shown in Fig.4.10. The current through the sample can be calculated by:

$$I = \frac{V_{in} - V_{BE}}{R_{ref}} = \frac{V_{std}}{R_{std}}, \tag{4.2}$$

where, V_{in} is the voltage of the base and V_{BE} is the base-emitter bias of the transistor. The current as a function of time and voltage are displayed on Lecroy 9341A oscilloscope. The computer can monitor the oscilloscope, collect data and adjust the current.

Chapter 5

Data and Analysis

In this chapter, the results of the transport measurements of $NbTiN$ samples with different thicknesses is discussed.

$NbTiN Sample$

The original thickness of the $NbTiN$ sample that we have used is 125 nm thickness and is an amorphous type. All superconducting $NbTiN$ films with different thicknesses were initially DC tested (using 4-probe measurement technique) with and without an applied magnetic field. The Cryomech $PT405$ Cryostat was the main system that we have used for doing all of our measurements.

First thing after we put the sample in is to cool down the system and a measurement called Free Fall. While cooling down the system, we record the change of resistance versus temperature. Graphing that can give us a rough estimate of how much critical temperature and normal resistivity is which might be helpful later on. Plus the process of cooling down is needed to be done regardless.

The onset T_c is defined as the intersection of the extrapolation of the normal-state portion and the extrapolation of the steep transition portion of the $R(T)$ curve [30]. The applied magnetic field in our measurements is in both parallel and perpendicular orientations. We try to have a high point density in our measurements, in order to have more accurate graphs. The highest magnetic field that we can achieve with our magnet in our system is around 1.3 T and depending on the type of measurement that we are doing, we can have different steps for the magnetic field (we usually use

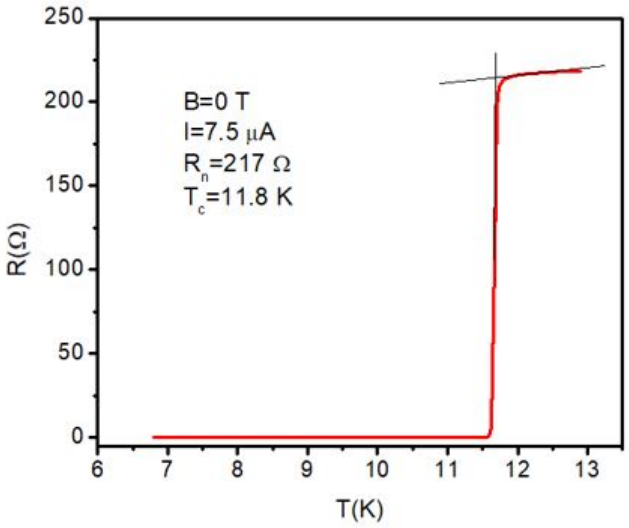

Figure 5.1: Critical temperature measurments of $NbTiN$ superconducting sample (125 nm thickness)

0.1 T steps). We try to find the values of important superconductivity parameters like coherence length, effective coherence length, penetration depth, superconducting electron density and also critical boundaries like critical temperature, magnetic field and depairing current. We repeat our measurements for different thicknesses of $NbTiN$ superconducting films (125 nm, 83 nm and 37 nm) to see how important superconducting parameters are changing based on the thickness of the films. We have achieved different thicknesses for our thin films by milling them down in our ion milling machine. We have calculated the milling rate with our ion gun machine to be 0.189 nm/min.

Measurements on the first thickness of $NbTiN$ superconducting sample

Based on our measurements, this $NbTiN$ superconducting film is a type II superconductor with a transition of around 0.5 K and critical temperature around of 11.8 K (Fig.5.1). The normal resistance for this film thickness is 217 Ω with a resistivity

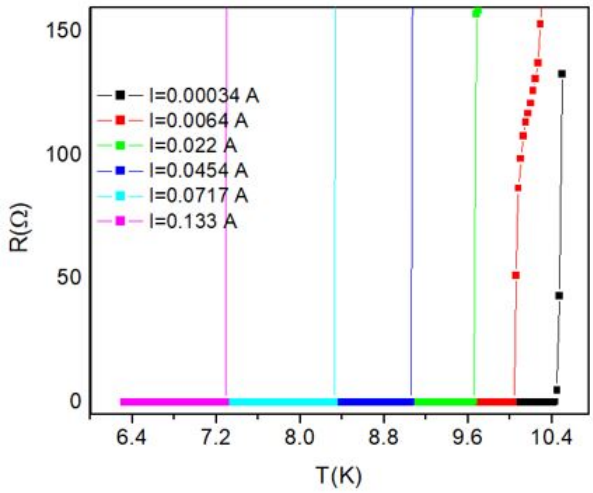

Figure 5.2: Resistive transitions for $NbTiN$ at zero magnetic field for different values of current of (right to left): 0.34 mA, 6.4 mA, 22 mA, 45.4 mA, 71.7 mA and 133 mA

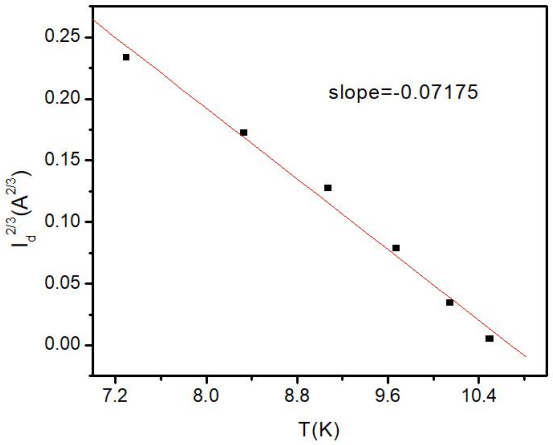

Figure 5.3: $I_d^{2/3}$ versus temperature values

of 1.37×10^{-6} Ωm.

In order to calculate the value of depairing current denisty $j_d(0)$, we first need to calculate the value of deparing current $I_d(0)$. Fig.5.2 shows the resistive transition at zero magnetic field for various applied currents. The lowest current value in this graph is 0.34 mA and the highest is 133 mA and all currents are pulsed. All the curves

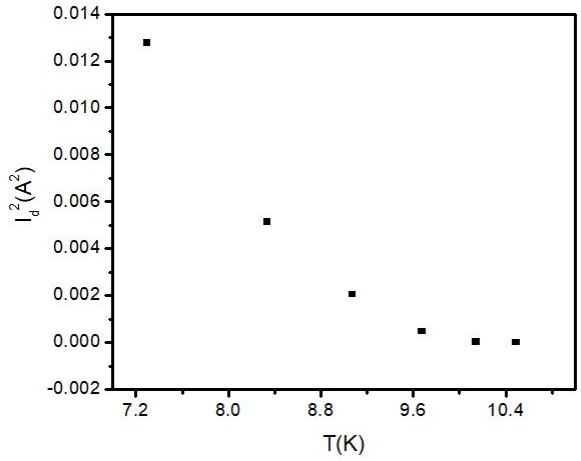

Figure 5.4: I_d^2 versus T graph

shift in a fairly parallel manner over the central portion of the normal resistance ($R \approx R_n/2$). The depairing current value $I_d(T)$ at different values of T is defined at the midpoint of the resistive transition $R = R_n/2 = 108.5\ \Omega$. Fig. 5.3 shows the values of $I_d^{2/3}$ points against T (corresponding to the pair breaking effect). The two third power graph is confirming the induced depairing current phenomenon in GL theory. By the values of y-axis intercept of the $I_d^{2/3}(T)$ versus the temperature graph, we can find the zero temperature value to be $I_d(0) \approx 0.25[T_c dI^{2/3}/dT]^{3/2}$ [33]. Based on our results in Fig.5.3 the value of $I_d(0) = 195.8mA$. We also need to make sure that our heat removal from the sample is effective. In order to do so, we are making sure there is no shift in the temperature due to joule heating ($I_d^2 \propto \rho j^2$). By graphing the value of I_d^2 versus T we see that by increasing the temperature the value of I_d^2 does not increase linearly which is a confirmation of the fact that the Joule heating here is negligible (Fig.5.4). Now We can say the shift in the temperature is only due to the depairing effect. We can calculate the depairing current density by dividing the value of depairing current ($I_d(0)$) by the sectional area of our sample ($A = width \times depth = 1.375 \times 10^{-12} m^2$). We report the corresponding value of depairing current density at zero-temperature to be $j_d(0) = 142.4 \times 10^9\ A/m^2$.

The value of depairing current densisty is related to the upper critical field B_{c2} and the magnetic penetration depth. Becuase $B_{c2}(T, j)$ is a function of current as well, we obtain the value of the B_{c2} for our sample by measuring the shift in the resistive transition by applying different magnetic fields at a constant low current value. Resistive transition of $NbTiN$ sample for 7.5 μA in perpendicular magnetic field is shown in Fig.5.5. The information from these curves was used to determine the value of upper critical field (B_{c2}). In order to do so, we use the results of resistance versus tempreture graph and we find the temperatures corresponding to the midpoint of resistance transition. By defining B_{c2} at the midpoint of the transition ($B_{c2}(T)$) in Fig. 5.6, the value of $B_{c2}(0)$ can be calculated. It was shown before by Werthamer et al. [44] that $B_{c2}(0) \approx 0.7 T_c dB_{c2}(T)/dT$ and is known as WHH formalism. The value of $B_{c2}(0)$ for our sample in perpendicular magnetic field is calculated to be 12.05 T by use of WHH formalism.

By the information that we have on the upper value of magnetic field, we extract the value of coherence length by use of $B_{c2} = \Phi_0/2\pi\xi^2$ formula. We report the coherence length ξ of our sample for this thickness in perpendicular magnetic field to be equal to 5.23 nm. This value of ξ that is deduced from the upper critical field can be reduced by the scattering, and is a macroscopic value. There is another coherence length value that is called intrinsic BCS coherence length ξ_0 that is not depending on the scattering and is a microscopic value. These two values are related by $\xi \approx \sqrt{\xi_0 l}$, where l is the mean free path of electrons [20]. In our case as scattering is in all 3 directions of our sample, and we are changing the thickness only, the value of ξ can be proportional to the thickness ($\xi \approx \sqrt{\xi_0 d}$). By the information that we have on ξ and thickness of our sample d, We report the value of in plane ξ_0 to be ~ 0.2 nm.

The combination of values of depairing current density and upper critical field provide a useful method for obtaining the value of penetration depth (λ) purely from transport measurements. This value of λ is an absolute value and is unaffected by

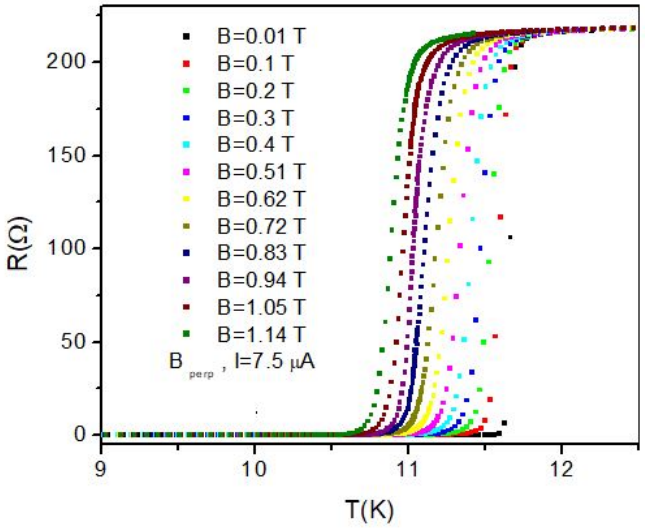

Figure 5.5: Resistive transitions for $NbTiN$ at a current of I=7.5 μA in perpendicular magnetic field values of (right to left): 0.01 T, 0.1 T, 0.2 T, 0.3 T, 0.4 T, 0.51 T, 0.62 T, 0.72 T, 0.83 T, 0.94 T, 1.05 T, 1.14 T

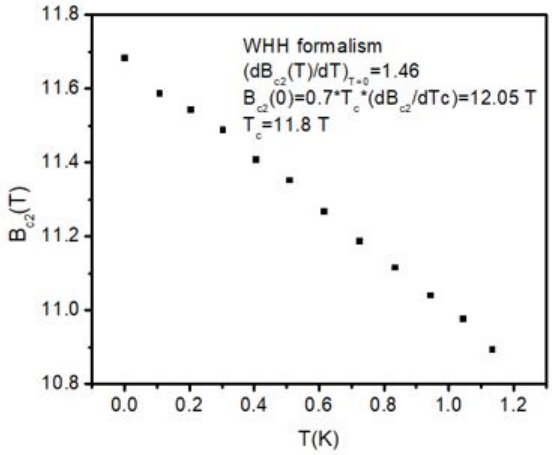

Figure 5.6: Upper critical magnetic field versus the midpoint transition temperature for perpendicular magnetic field

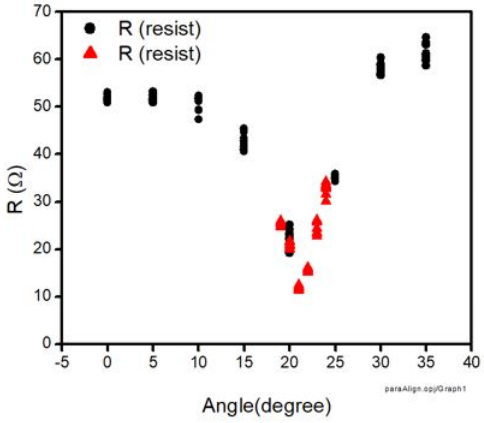

Figure 5.7: The allignemt measurements in order to find the angle where resistance is minimum which is at 21.3 degree

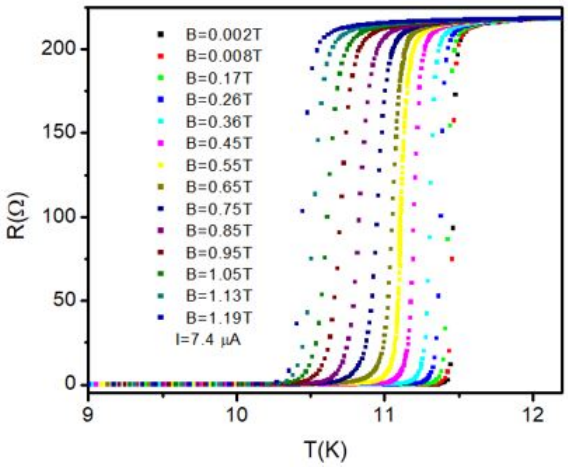

Figure 5.8: Resistive transitions for $NbTiN$ sample at a current of I=7.4 μA in parallel magnetic field values of (right to left): 0.002, 0.008, 0.17, 0.26, 0.36, 0.45, 0.55, 0.65, 0.75, 0.85, 0.95, 1.05, 1.13, 1.19 T

magnetism in material [30]. This value is calculated to be equal to 0.368 μm and we report the value of $\kappa = \lambda/\xi = 70.36$, which puts this material in the extreme superconducting category. We now utilize the information obtained about λ to estimate the carrier concentration value from $n_s = m^*/4\mu_0 e^2\lambda^2$ formula. Assuming that the effective electron mass m^* equals the free electron mass, m, e is the electron charge, we get the density of superconducting electrons density n_s to be 2.092×10^{26} m^{-3}.

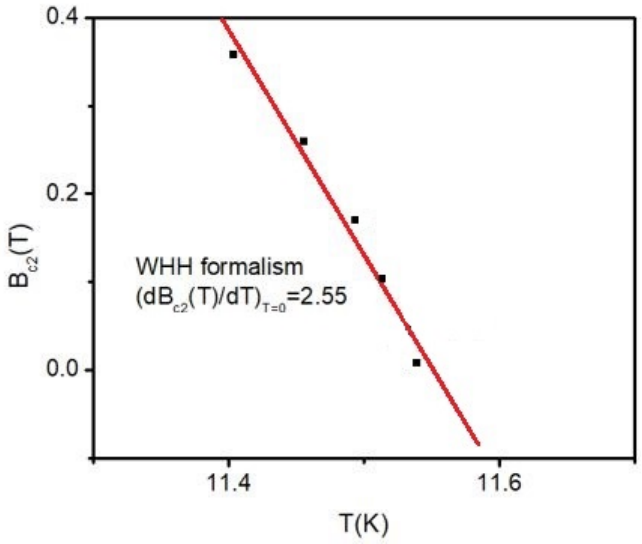

Figure 5.9: Upper critical magnetic field versus the midpoint transition temperature for parallel magnetic field

We have repeated the measurement in the parallel magnetic field as well. For having the magnetic field being parallel to our sample, we need to do the alignment as when we put it in the system the orientation can not be exactly parallel. We measure the value of resistance at highest magnetic field that we have (1.3 T) at different angles and then we graph $R(\theta)$ to find the angle that gives us the minimum value of the resistance. Because in parallel orientation, the flux penetration is minimum. As it is shown in Fig.5.7 we can see 21.3 degree is the minimum of our $R(\theta)$ graph. Then we graph the change of resistance versus temperature at different magnetic field steps (0.002, 0.008, 0.17, 0.26, 0.36, 0.45, 0.55, 0.65, 0.75, 0.85, 0.95, 1.05, 1.13, 1.19 T) in order to find the parallel upper critical field Fig.5.8. The value of B_{c2} by WHH formalism is 21.06 T Fig.5.9. The coherence length value for parallel magnetic field is ξ=3.96 nm, BCS coherence length value is $\sim$ 0.1 nm and λ=0.423 μm. The GL parameter value for this thickness is $\kappa = \lambda/\xi = 106.98$.

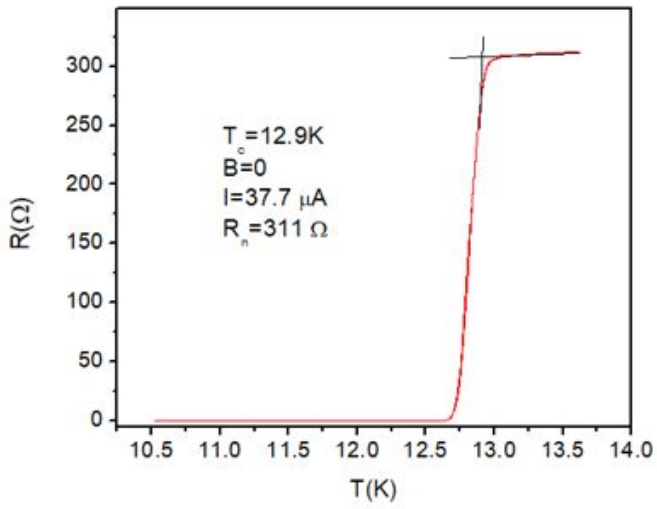

Figure 5.10: Critical tempreture measurments of $NbTiN$ superconducting sample after first thining

Measurements on the second thickness of $NbTiN$ superconducting sample

After putting our sample in ion milling machine and milling it down for 3 hours and 40 min (with milling rate of $\sim 11.36nm/hr$), our film thickness is measured to be 83 nm. This thickness is 66.4 % of original thickness of the film. As it can be seen from Fig.5.10, the normal resistance value increases to 311Ω. The value of T_c also increases to $12.9K$ which is almost $\sim 1K$ higher than the first thickness. We have done the depairing current density measurements based on resistance versus temperature measurements in zero magnetic field for different pulsed current values ranging between 0.33 mA to 4.6 mA as shown in Fig.5.11. After finding the values of $I_d(T)$ based on the midpoint of transition cuts and making sure that Joule heating is negligible (Fig. 5.12) we were able to find the value of $I_d(0)$ by the result of the slope of Fig.5.21 to be equal to 128.68 mA. For this thickness the value of $j_d(0) = 140.94 \times 10^9$ A/m^2. Compared to the first thickness this value does not change much.

The measurements of change of resistance versus temperature for different mag-

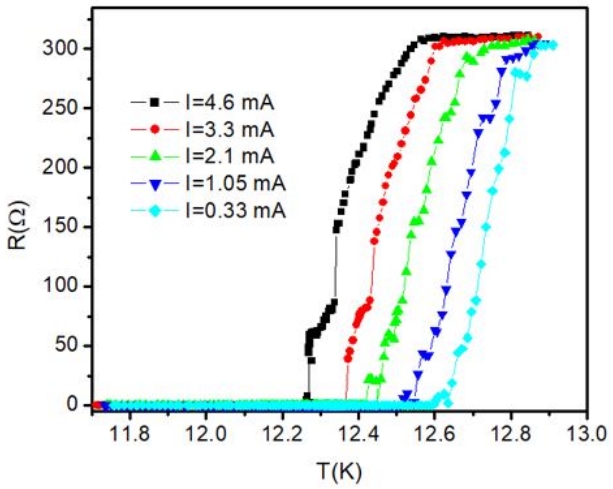

Figure 5.11: Resistive transitions for $NbTiN$ at zero magnetic field for different values of current of (right to left): 0.33 mA, 1.05 mA, 2.1 mA, 3.3 mA and 4.6 mA

netic fields (in perpendicular orientation) at different magnetic field steps (0, 0.12, 0.24, 0.36, 0.48, 0.60, 0.72, 0.88, 1, 1.12, 1.20 T) is shown in Fig.5.14 at a constant current of 37 μA. Like before, we do the 50% of resistance cut and then we obtain the values of $B_{c2}(T)$ for the midpoint transition. After graphing the values of $B_{c2}(T)$ and use of WHH formalism we report the value of upper critical field be equal to 17.61 T (Fig.5.15), which is higher than the first film. By the information on upper magnetic field and depairing current density, we are able to find the value of coherence length coherence length ξ in perpendicular magnetic field to be equal to 4.32 nm, $\xi_0 \sim 0.2$ nm, $\lambda \simeq 0.406$ μm, $n_s \simeq 1.71 \times 10^{26}$ m^{-3} and $\kappa = \lambda/\xi = 93.98$. We see a decrease in the value of coherence length and an increase in the value of magnetic penetration depth. Both values of n_s and ξ_0 are staying almost the same.

For the parallel orientation, we have graphed the change of resistance versus temperature at different magnetic field steps (0, 0.12, 0.24, 0.36, 0.48, 0.60, 0.78, 0.9, 1.02, 1.11, 1.23) at constant current of 26 μA in order to find the parallel upper critical field (Fig.5.16). The value of B_{c2} by WHH formalism is 47.40 T based on the slope of Fig. 5.17. This value is increasing compared to the previous thickness.

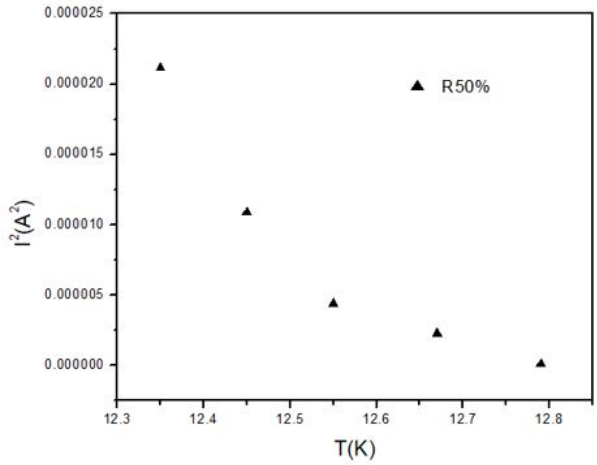

Figure 5.12: I_d^2 versus T graph

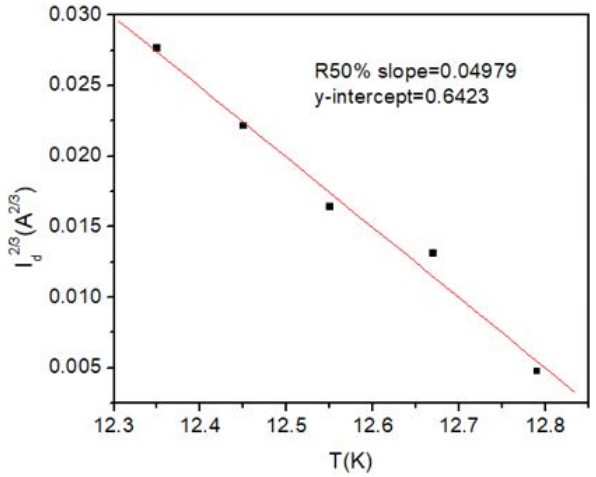

Figure 5.13: $I_d^{2/3}$ versus temperature in order to find the value of depairing current

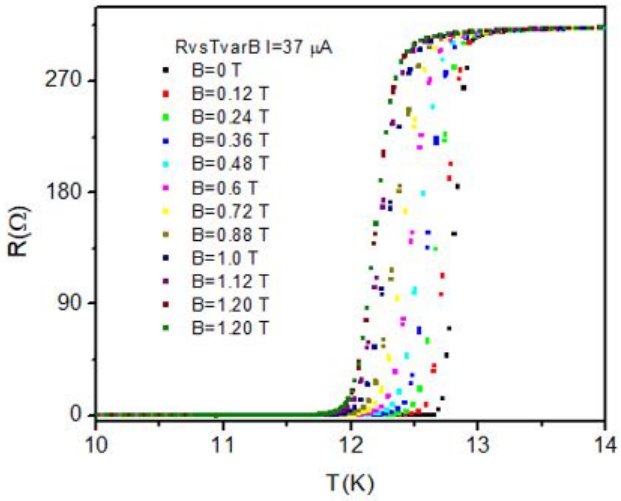

Figure 5.14: Resistive transitions for $NbTiN$ at a current of I=37 μA in perpendicular magnetic field values of (right to left): 0, 0.12, 0.24, 0.36, 0.48, 0.60, 0.72, 0.88, 1, 1.12, 1.20 T

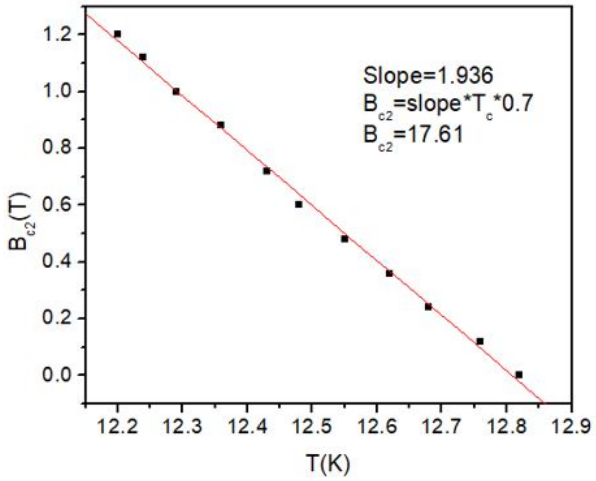

Figure 5.15: The value of B_{c2} by WHH formalism which is 17.61 T

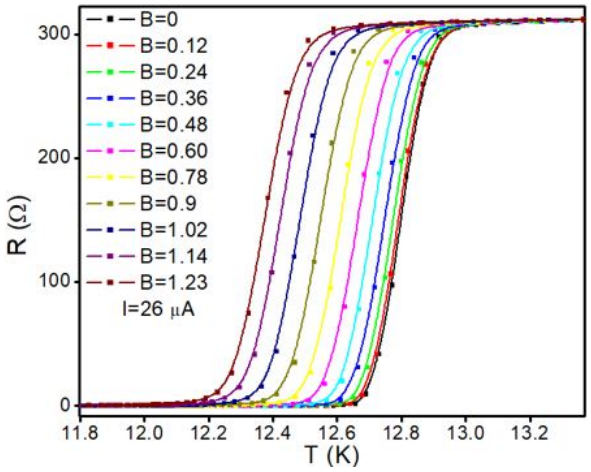

Figure 5.16: Resistive transitions for $NbTiN$ at a current of I=26 μA in parallel magnetic field values of (right to left): 0, 0.12, 0.24, 0.36, 0.48, 0.60, 0.78, 0.9, 1.02, 1.11, 1.23 T

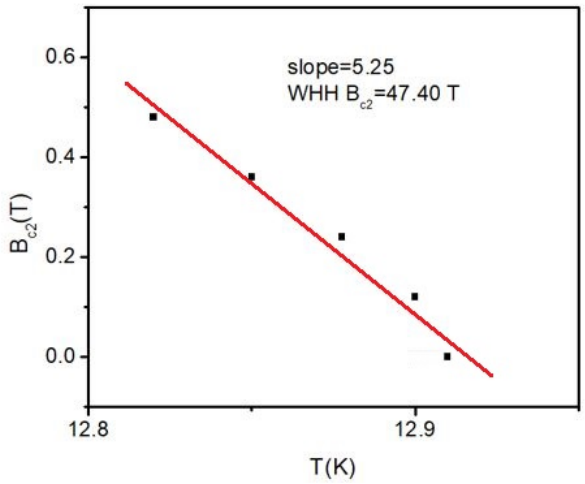

Figure 5.17: The value of B_{c2} by WHH formalism which is 47.40 T

The coherence length value for parallel magnetic field is $\xi = 2.63\ nm$, BCS coherence length value is $\sim 0.1\ nm$ and λ= 0.521 μm. The GL parameter value for this thickness in parallel magnetic field orientation is $\kappa = \lambda/\xi = 198$. By decreasing the thickness, we see an increase in the value of penetration depth and a decrease in the value of coherence length. The value of BCS coherence length is not changing.

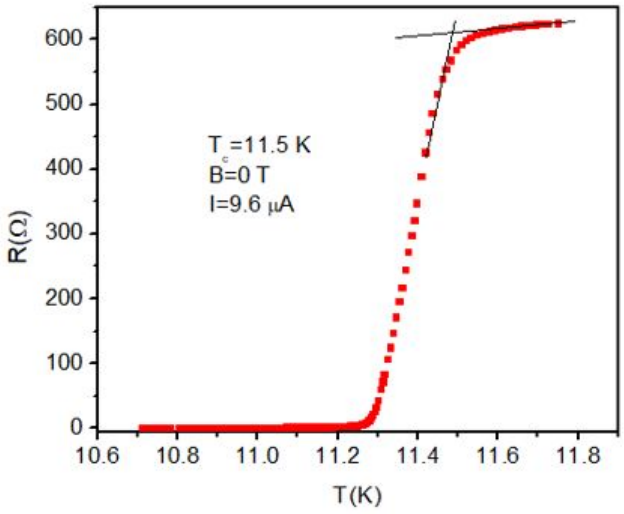

Figure 5.18: Critical tempreture measurments of $NbTiN$ superconducting sample after second thining

Measurements of the third thickness of $NbTiN$ superconducting sample

After putting our sample for the second time in ion milling machine and milling it down for extra 4 hours and 1 min with the previous milling rate), we get to the third thickness of our sample which is 37 nm. The thickness of the film at this point is 29.08 % of the original thickness of the film. As it can be seen from Fig. 5.18 the normal resistance is increasing to 624 Ω which is almost double as the previous thickness. The value of T_c here is decreasing to 11.5 K which is closer to the T_c of the first thickness.

We have done the depairing current density measurements based on resistance versus temperature measurements in zero magnetic field for different pulsed current values between 4.9 mA to 63 mA for this thickness is shown in Fig.5.19. Similar to the previous situations, we can find the values of $I_d(T)$ based on the midpoint of transition cuts and also making sure that Joule heating is negligible (Fig.5.20), we

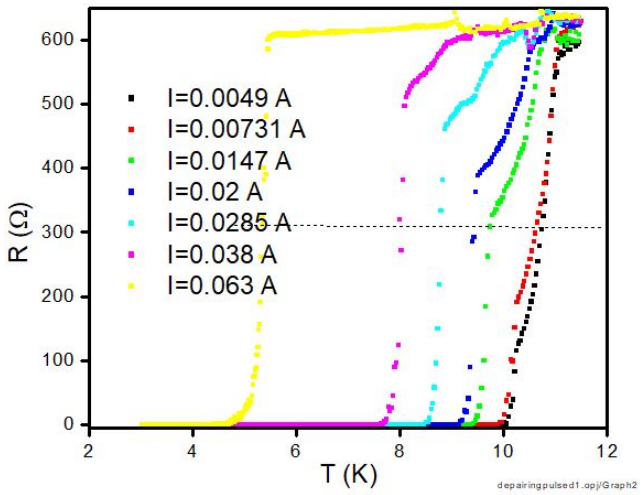

Figure 5.19: Resistive transitions for $NbTiN$ at zero magnetic field for different values of current of (right to left): 4.9 mA, 7.31 mA, 14.7 mA, 20 mA, 28.5 mA, 38 mA and 63 mA

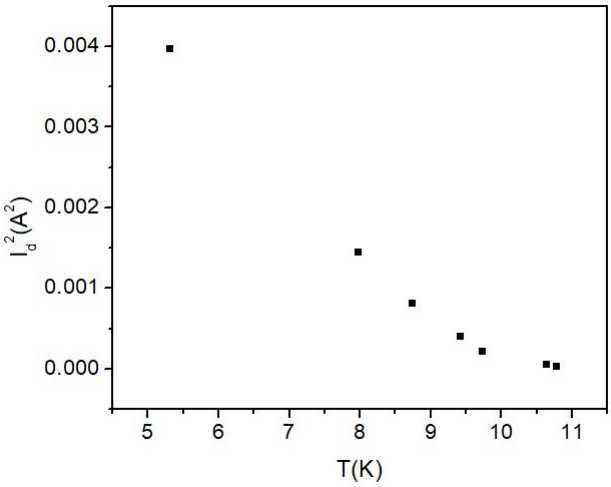

Figure 5.20: I_d^2 versus T graph

were able to find the value of $I_d(0)$ by the result of the slope of Fig. 5.21. The value of $I_d(0)$ is 144 mA gives us the value of $j_d(0) = 351.2 \times 10^9 A/m^2$ which is a lot higher than the other two thicknesses.

The measurements of change of resistance versus temperature for different magnetic fields (in perpendicular orientation) at different magnetic field steps (0, 0.1,

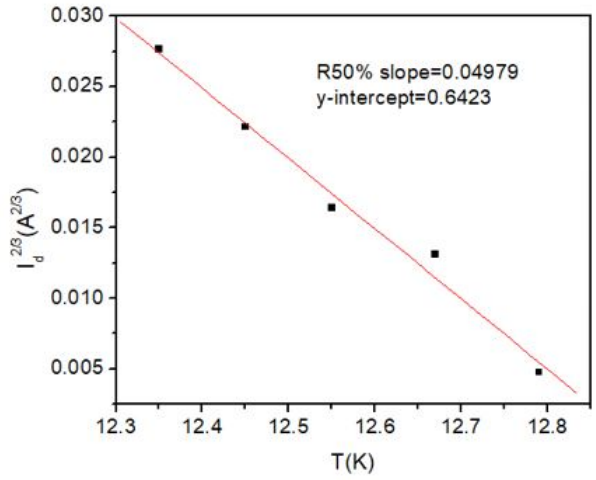

Figure 5.21: $I_d^{2/3}$ versus temperature in order to find the value of depairing current

0.22, 0.34, 0.46, 0.58, 0.84, 0.88, 0.97, 1.08 T) is shown in Fig.5.22 at a constant current of 9.6 μA. Like before, we do the 50 % of resistance cut and then we obtain the values of $B_{c2}(T)$ for the midpoint transition. After graphing the values of $B_{c2}(T)$ versus T and use of WHH formalism we report the value of upper critical field be equal to 43.23 T (Fig.5.23), which is increasing compared to the other two thicknesses. The coherence length value for this thickness and perpendicular magnetic field orientation is $\xi = 2.71\ nm$, BCS coherence length value is $\sim 0.2\ nm$ and λ= 0.340 μm. The GL parameter value for this thickness is $\kappa = \lambda/\xi = 125.46$ and the value of superconducting electrons density is $n_s = 2.45 \times 10^{26}\ m^{-3}$. By decreasing the thickness we can see a decrease in the value of penetration depth compare to the other two thicknesses.

Table 5.1 is showing different superconducting parameters such as critical temperature, upper critical magnetic field and depairing current density values in perpendicular magnetic filed for different thicknesses to give us a summery of all of these values and change of them based on the thickness. Other groups such as Matsunaga et al. [35] have calculated the value of T_c to be 15 K or lower that can be depending on the

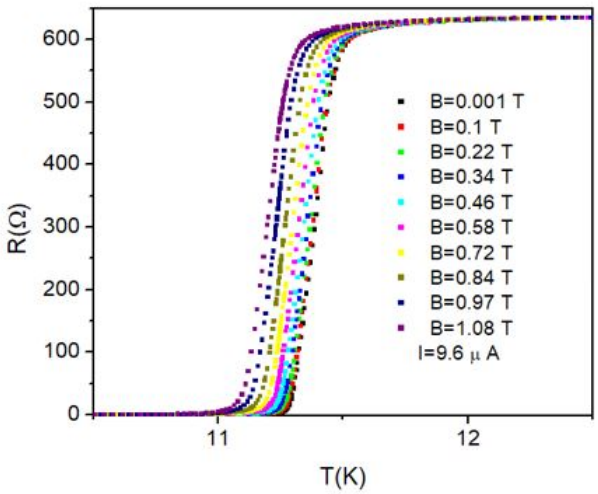

Figure 5.22: Resistive transitions for $NbTiN$ at a current of I=9.6 μA in the perpendicular magnetic field values of (right to left): 0, 0.1, 0.22, 0.34, 0.46, 0.58, 0.84, 0.88, 0.97, 1.08 T

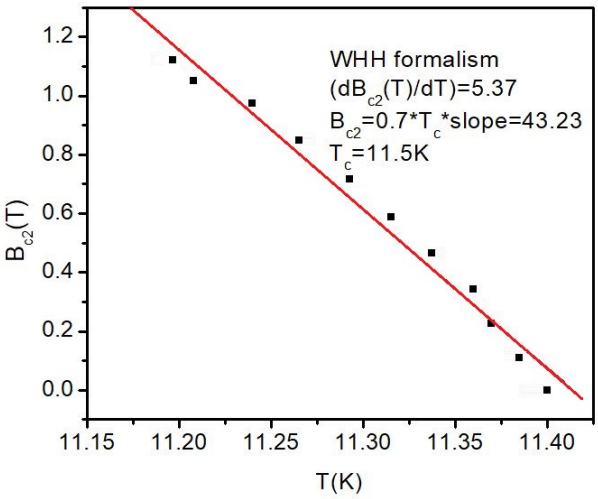

Figure 5.23: The value of B_{c2} by WHH formalism which is 43.23 T

Table 5.1: Values of R(Ω), $j_d(0)(A/m^2)$, $T_c(K)$, $B_{c2}(T)$, $\xi(nm)$, $\xi_0(nm)$, $\lambda(\mu m)$, κ and $n_s(m^{-3})$ for perpendicular magnetic field orientation for three different thicknesses of $NbTiN$ superconducting films

t (nm)	R (Ω)	$j_d(0)$ (A/m^2)	T_c (K)	B_{c2} (T)	ξ (nm)	ξ_0 (nm)	λ (μm)	κ	n_s (m^{-3})
125	217	142.4×10^9	11.8	12.05	5.23	0.2	0.368	70.36	2.092×10^{26}
83	311	140.94×10^9	12.9	17.61	4.32	0.2	0.406	93.98	1.71×10^{26}
37	624	351.21×10^9	11.5	43.23	2.71	0.2	0.340	125.46	2.45×10^{26}

thickness of the film or substrates. Our experimental values for all three thicknesses is in agreement with their results. Lei Yu et al. [45] seen an increase in the value of critical temperature, by increasing the thickness and the decrease of penetration depth. We have not seen any type of trend (increasing or decreasing) in the value of critical temperature, which can be due to the fact that our sample is amorphous type unlike other groups. We also have seen a decrease in the value of penetration depth which is in agreement with Lei Yu et al. experimental results. The value of resistance and upper critical field is increasing by decreasing the thickness that can be due to the increase in the scattering and disorder by thinning down our sample. We get the same value of ξ_0 for all three thicknesses as we expect, which should be independent of geometry of the sample. The value of superconducting density for all three thicknesses is almost the same, which is what is expected as it is a density value and should be independent of the thickness.

For the parallel orientation, we have graphed the change of resistance versus temperature at different magnetic field steps (0, 0.109, 0.225, 0.343, 0.464, 0.588, 0.716, 0.847, 0.974, 1.087, 1.2 T) in order to find the parallel upper critical field for a constant current of 9.6 μA (Fig.5.24). The value of B_{c2} by WHH formalism is 92.17 T based on the slope of Fig. 5.25. The coherence length value for parallel magnetic field is $\xi = 1.89\ nm$, BCS coherence length value is $\sim 0.1\ nm$ and $\lambda = 0.389\ \mu m$.

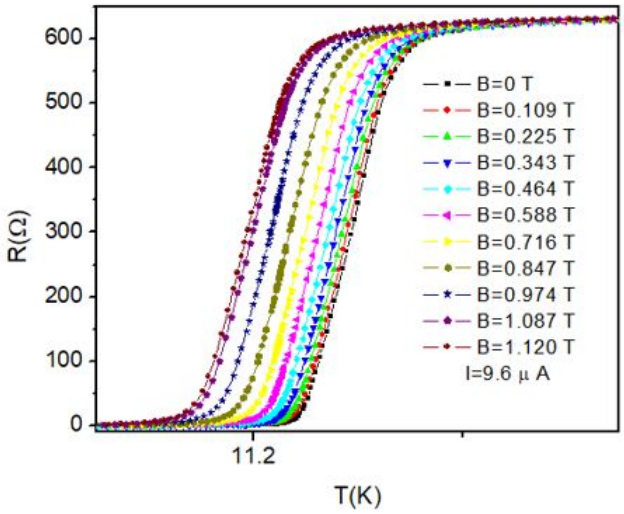

Figure 5.24: Resistive transitions for $NbTiN$ at a current of I=9.6 μA in parallel magnetic field values of (right to left): 0, 0.109, 0.225, 0.343, 0.464, 0.588, 0.716, 0.847, 0.974, 1.087, 1.2 T

Table 5.2: Values of $B_{c2}(T)$, $\xi(nm)$, $\xi_0(nm)$, $\lambda(\mu m)$ and κ for parallel magnetic field orientation for three different thicknesses of $NbTiN$ superconducting films

t (nm)	B_{c2} (T)	ξ (nm)	ξ_0 (nm)	λ (μm)	κ
125	21.06	3.96	0.1	0.423	106.89
83	47.40	2.63	0.1	0.521	198
37	92.17	1.89	0.1	0.389	205.82

The GL parameter value for this thickness is $\kappa = \lambda/\xi = 205.82$.

Table 5.2 is showing different superconducting parameters, critical temperature, upper critical magnetic field and depairing current density values in parallel magnetic filed for different thicknesses of $NbTiN$ films. By decreasing the thickness of the film, we see an increase in the value of upper critical field in this magnetic field orientation as well. We see an decrease in the value of coherence length. We also get the same value of ξ_0 for all three thicknesses as we expect.

All our experimental data was compared with the calculated ones from the existing theories and, other groups experimental values. For both orientations of magnetic

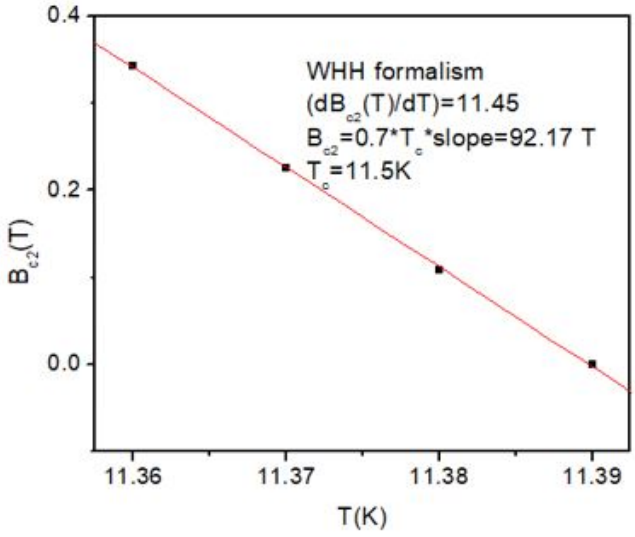

Figure 5.25: The value of B_{c2} by WHH formalism which is 92.17 T

field, We have seen critical field $B_{c2}(T)$ functions conform to GL predictions. We were not able to find any value in the literature for the depairing current density values provided by other groups for this type of superconductor, but our results is in the range that is expected for all other type of superconductors. We also have observed that $j_d(T)$ function confrom to GL predictions. With the result of our depairing current density measurements, we were able to find the exact value of magnetic penetration depth. Other groups such as Hu et al. [16] have calculated the value of λ to be in the range of $200 - 400$ nm which is in agreement with all of our experimental results. The values of κ for all different thicknesses put this material in the range of extreme superconducting material.

Chapter 6

Conclusions

In the present work we investigated the superconducting properties of $NbTiN$ superconducting films with different thicknesses. In particular, we have studied the upper-critical-field and current induced effect. Both $j_d(T)$ and $B_{c2}(T)$ functions, conform to GL predictions. The measurements of $j_d(T)$ and $B_{c2}(T)$ combined, provide a useful method to obtain λ based on transport measurements. This is of special value in the situations in which the geometry of the sample or the volume makes it not suitable for the penetration depth measurements by inductive methods. By decreasing the thickness we see an increase in the value of $B_{c2}(0)$, which can be due to the fact that scattering and effective disorder are increasing. The values of T_c and λ for all different films were in agreement with other groups. The values of ξ_0 and n_s are constant for different thicknesses, which is in agreement with what is expected.

Bibliography

[1] S. Kazeminasab A. Amerinatanzi A. Hadi, K. Alipour and M. Elahinia, *Asme proceedings | integrated system design and implementation*, ASME Proceedings | Integrated System Design and Implementation **1** (2016).

[2] AA Abrikosov, *Nobel lecture: Type-ii superconductors and the vortex lattice*, Reviews of modern physics **76** (2004), no. 3, 975.

[3] Amirhesam Amerinatanzi, Rodney K. Summers, Kaveh Ahmadi, Vijay K. Goel, Timothy E. Hewett, and Edward Nyman, *Automated measurement of patient-specific tibial slopes from mri*, Bioengineering **4** (2017), 69.

[4] Igor S. Aranson and Lorenz Kramer, *The world of the complex ginzburg-landau equation*, Rev. Mod. Phys. **74** (2002), 99–143.

[5] John Bardeen, Leon N Cooper, and J Robert Schrieffer, *Theory of superconductivity*, Physical Review **108** (1957), no. 5, 1175.

[6] John Bardeen and M. J. Stephen, *Theory of the motion of vortices in superconductors*, Phys. Rev. **140** (1965), A1197–A1207.

[7] R Barends, HL Hortensius, T Zijlstra, JJA Baselmans, SJC Yates, JR Gao, and TM Klapwijk, *Noise in nbtin, al, and ta superconducting resonators on silicon and sapphire substrates*, Applied Superconductivity, IEEE Transactions on **19** (2009), no. 3, 936–939.

[8] J. G. Bednorz and K. A. Muller, *Possible hight c superconductivity in the ba-la-cu-o system*, Zeitschrift für Physik B Condensed Matter **64** (1986), no. 2, 189–193.

[9] Thomas W Cecil, Robert M Weikle, Anthony R Kerr, and Arthur W Lichtenberger, *Investigation of nbtin thin films and aln tunnel barriers with ellipsometry for superconducting device applications*, Applied Superconductivity, IEEE Transactions on **17** (2007), no. 2, 3525–3528.

[10] Leon N Cooper, *Bound electron pairs in a degenerate fermi gas*, Physical Review **104** (1956), no. 4, 1189.

[11] EFC Driessen, PCJJ Coumou, RR Tromp, PJ De Visser, and TM Klapwijk, *Strongly disordered tin and nbtin s-wave superconductors probed by microwave electrodynamics*, Physical review letters **109** (2012), no. 10, 107003.

[12] W. Farrell Edwards, *Classical derivation of the london equations*, Phys. Rev. Lett. **47** (1981), 1863–1866.

[13] Herbert Fröhlich, *Theory of the superconducting state. i. the ground state at the absolute zero of temperature*, Physical Review **79** (1950), no. 5, 845.

[14] Rodney K. Summers; Amirhesam Amerinatanzi; Timothy E. Hewett; Edward Nyman; Vijay K. Goel, *Novel measurement of multi-planar proximal tibial slope*, Medicine & Science in Sports & Exercise (2016).

[15] Lev Petrovich GorâĂŹkov, *Microscopic derivation of the ginzburg-landau equations in the theory of superconductivity*, Sov. Phys. JETP **9** (1959), no. 6, 1364–1367.

[16] R. Hu, G. L. Kerber, J. Luine, E. Ladizinsky, and J. Bulman, *Sputter deposition conditions and penetration depth in nbn thin films*, IEEE Transactions on Applied Superconductivity **13** (2003), no. 2, 3288–3291.

[17] XQ Jia, L Kang, XZ Yang, ZH Wang, TK Ren, BB Jin, Jiann-Jong Chen, WW Xu, and PH Wu, *Ultrathin nbtin films with high ti composition for superconducting nanowire single photon detectors*, Applied Superconductivity, IEEE Transactions on **25** (2015), no. 3, 1–4.

[18] Jonathan Kawamura, Jian Chen, David Miller, Jacob Kooi, Jonas Zmuidzinas, Bruce Bumble, Henry G. LeDuc, and Jeff A. Stern, *Low-noise submillimeter-wave nbtin superconducting tunnel junction mixers*, Applied Physics Letters **75** (1999), no. 25, 4013–4015.

[19] James M. Knight and Milind N. Kunchur, *Energy relaxation at a hot-electron vortex instability*, Phys. Rev. B **74** (2006), 064512.

[20] Milind Kunchur, *Current-induced pair breaking in magnesium diboride*, Journal of Physics: Condensed Matter **16** (2004), no. 39, R1183.

[21] Milind N Kunchur, *Novel transport behavior found in the dissipative regime of superconductors*, Modern Physics Letters B **9** (1995), no. 07, 399–426.

[22] Milind N. Kunchur, *Unstable flux flow due to heated electrons in superconducting films*, Phys. Rev. Lett. **89** (2002), 137005.

[23] Milind N. Kunchur, David K. Christen, Charles E. Klabunde, and Julia M. Phillips, *Pair-breaking effect of high current densities on the superconducting transition in* $\mathrm{yba_2cu_3o_{7-\delta}}$, Phys. Rev. Lett. **72** (1994), 752–755.

[24] Milind N. Kunchur, Charles Dean, Manlai Liang, Nahid S. Moghaddam, Anita Guarino, Angela Nigro, Gaia Grimaldi, and Antonio Leo, *Depairing current density of nd2âĹŠxcexcuo4âĹŠÎt superconducting films*, Physica C: Superconductivity **495** (2013), 66 – 68.

[25] Milind N Kunchur and Knight James, *Hot-electron instability in superconductors*, Mod. Phys. Lett (2003).

[26] Milind N. Kunchur, Sung-Ik Lee, and W. N. Kang, *Pair-breaking critical current density of magnesium diboride*, Phys. Rev. B **68** (2003), 064516.

[27] Milind N Kunchur, Manalai Liang, and A Gurevich, *The vortex explosion transition*, Solid state physics: Proceeding of the 57th DAE solid state physics symposium, vol. 1512, AIP Publishing, 2013, pp. 19–21.

[28] Milind N. Kunchur and S. J. Poon, *Critical fields and critical currents of superconducting disks in transverse magnetic fields*, Phys. Rev. B **43** (1991), 2916–2921.

[29] M.N. Kunchur, D.K. Christen, and B.I. Ivlev, *Transport behavior in superconductors at extreme dissipation levels*, (1996).

[30] MN Kunchur, CL Dean, N Shayesteh Moghadam, JM Knight, QL He, H Liu, J Wang, R Lortz, IK Sou, and A Gurevich, *Current-induced depairing in the bi 2 te 3/fete interfacial superconductor*, Physical Review B **92** (2015), no. 9, 094502.

[31] M Kupriyanov, KK Likharev, and VF Lukichev, *Influence of effective electron interaction on critical current of josephson weak links*, Sov. Phys. JETP **56** (1982), no. 1, 235–240.

[32] Lev Davidovich Landau and VL Ginzburg, *On the theory of superconductivity*, Zh. Eksp. Teor. Fiz. **20** (1950), 1064.

[33] Manlai Liang, Milind N. Kunchur, L. Fruchter, and Z.Z. Li, *Depairing current density of infinite-layer sr1âĹŠxlaxcuo2 superconducting films*, Physica C: Superconductivity **492** (2013), 178 – 180.

[34] F. London and H. London, *The electromagnetic equations of the supraconductor*, Proceedings of the Royal Society of London A: Mathematical, Physical and Engineering Sciences **149** (1935), no. 866, 71–88.

[35] T. Matsunaga, H. Maezawa, and T. Noguchi, *Characterization of nbtin thin films prepared by reactive dc-magnetron sputtering*, IEEE Transactions on Applied Superconductivity **13** (2003), no. 2, 3284–3287.

[36] Karl-Hubert Mess, Siegfried Wolff, and Peter Schmüser, *Superconducting accelerator magnets*, World Scientific, 1996.

[37] Chandra M Natarajan, Michael G Tanner, and Robert H Hadfield, *Superconducting nanowire single-photon detectors: physics and applications*, Superconductor Science and Technology **25** (2012), no. 6, 063001.

[38] CA Reynolds, B Serin, and LB Nesbitt, *The isotope effect in superconductivity. i. mercury*, Physical Review **84** (1951), no. 4, 691.

[39] Gabriel F. Saracila and Milind N. Kunchur, *Ballistic acceleration of a supercurrent in a superconductor*, Phys. Rev. Lett. **102** (2009), 077001.

[40] Bernd Seeber, *Handbook of applied superconductivity*, vol. 2, CRC press, 1998.

[41] Tatsuya Shiino, Shoichi Shiba, Nami Sakai, Tetsuya Yamakura, Ling Jiang, Yoshinori Uzawa, Hiroyuki Maezawa, and Satoshi Yamamoto, *Improvement of the critical temperature of superconducting nbtin and nbn thin films using the aln buffer layer*, Superconductor Science and Technology **23** (2010), no. 4, 045004.

[42] JA Stern, B Bumble, HG LeDuc, JW Kooi, and J Zmuidzinas, *Fabrication and dc-characterization of nbtin based sis mixers for use between 600 and 1200 ghz*, Proc. 9th Int. Symp. Space THz Technol, Pasadena, CA, 1998, pp. 305–313.

[43] Michael Tinkham, *Introduction to superconductivity*, Courier Corporation, 1996.

[44] NR Werthamer, Ef Helfand, and PC Hohenberg, *Temperature and purity dependence of the superconducting critical field, h c 2. iii. electron spin and spin-orbit effects*, Physical Review **147** (1966), no. 1, 295.

[45] Lei Yu, R. K. Singh, Hongxue Liu, S. Y. Wu, R. Hu, D. Durand, J. Bulman, J. M. Rowell, and N. Newman, *Fabrication of niobium titanium nitride thin films with high superconducting transition temperatures and short penetration lengths*, IEEE Transactions on Applied Superconductivity **15** (2005), no. 1, 44–48.

[46] L Zhang, W Peng, LX You, and Z Wang, *Superconducting properties and chemical composition of nbtin thin films with different thickness*, Applied Physics Letters **107** (2015), no. 12, 122603.

Appendix A

Spinner Operation

In this section we discuss the operation of our spinner:

1. Turn on the power supplies of the spin coater and the compressor.

2. The outlet pressure of the compressor should be in the range of 60 $\sim$ 70 psi before starting.

3. Press "Select Process" and by using the up-down buttons, choose the preferred saved set up process. If you want to change the set up press "Edit Mode" and then "tab", then move the flashing cursor to the parameter that you want to change. You also always can create a new process based on what you need.

4. Press "Run Mode" to confirm the settings.

5. Open the lid and mount your desired vacuum chuck. If your sample is small, 3 mm chuck is a good choice, but if you are using a slide, a bigger chuck needs to be used.

6. Place the sample on top of the chuck and carefully try to align the center of the sample at the axial of the chuck.

7. Press "Vacuum" button now. If the compressor pressure is right, the vacuum reading on the screen should show a number between 17 to about 23.

8. Drip the photoresist on the top of the sample and make sure the whole surface of your sample is covered by that. You need to pay very careful attentions as chemicals should not get into the hole of the chuck as it may damage the motor.

9. Close the lid.

10. Make sure the LED light of the "Start" button is illuminating.

11. Press "Start" button. you should see the chuck starting to rotate right away. If for any reason you feel like something is wrong, press "Stop" at anytime.

12. Open the lid after it stops running.

13. Press "Vacuum" to drops that down to 0.

14. Take out the sample.

15. Put a protecting cap on the chuck and close the lid. Turn off both power supply and the compressor.

Appendix B

Sputtering machine operation

The following steps was followed in the deposition process:

1. Put the sample in sputtering machine and put the cap back on.
2. Make sure power supply is connected.
3. Turn on the rough pump connected to system and let it pump for a few minutes. Because it is a small sputtering machine, it does not need to be pumped for a long time.
4. Turn on the sputtering machine.
5. Watch the pressure indicator on the screen of the machine. You see the ready yellow light button on when the pressure gets to the desired pressure (around $10^{-}2\ mbar$).
6. Now turn argon gas on and wait a few minutes for the pressure to stabilize.
7. Make sure the timer on the machine is on 90 sec.
8. Press test button to see how much is the current that current indicator is showing (current should be in a range between 10 to 15 mA).
9. After you see the right current by testing, you can start sputtering by pressing start button.
10. Sputtering stops after 90 seconds, wait at least 30 seconds and repeat the process if you need to (better to wait longer than that).

11. Close argon gas.

12. Turn off the rough pump.

13. Turn off the sputtering machine.

14. Push up small knob on the top cap slowly to bring the pressure inside machine back to the room pressure.

15. Open the cap and take your sample out.

Appendix C

Operation for Oxford ion gun

In this section the operation of our ion milling machine is discussed:

1. Before you start make sure everything is at the off position and all the lid clamps are closed.

2. Put the sample inside the ion milling chamber at the marked position by matching the marker positions at both ends for mounting the gun head.

3. Turn the rough pump on.

4. Open the chamber rough valve slowly. It is safe to open the clamps when you see the pressure of chamber is less than 100 $torr$.

5. Open the green knob on the ion gun, when you see pressure is stabilized.

6. Close the chamber rough and gently open the turbo rough.

7. Switch the vacuum gauge to the turbo position and monitor it. Wait for it to drop under 20 $mtorr$.

8. Turn on the turbo pump. When you push the switch to "ON" and it goes back to the middle position. But you should see the yellow LED is on. After about 2 minutes, the green LED will be lit. This means the turbo pump is at its full speed.

9. Check the pressure of the chamber by switching back the vacuum gauge to chamber position to make sure it is still low.

10. Let it pump for about 20 minutes.

11. Slowly and carefully open high vacuum valve, while monitoring the turbo pressure on vacuum gauge. The pressure should not go over 100 $mtorr$. Wait for the pressure to stabilize.

12. Turn on cold cathode gauge and then press on and then number 1. This gauge shows the pressure of chamber which is usually in the order of $10^{-}5$ $torr$.

13. Set the flow control valve to be 6.1.

14. Make sure the low pressure gauge on argon gas tank is 10 psi.

15. Open the argon gas cylinder and switch the manifold very slowly making sure the turbo pressure does not go up. Wait for pressure to stabilize.

16. Turn on the power of the ion gun.

17. Adjust the beam current to be 100 μA with the beam energy less than 2.5 KeV.

18. Etching time depends on the desired thickness that we want and can take a few hours. It is better to take the sample after a few hours out and at some case it is needed to redo the lithography process.

19. When the ion milling is done, turn off the ion gun power supply. Close the gas cylinder and the flow valve.

20. Close the high vacuum valve.

21. Turn off turbo pump.

22. Do not turn off the rough pump at least for half an hour. Because the turbo cooling fan can keep the turbo bearing cool as the turbo spins down.

23. Close the turbo rough.

24. Turn off rough pump.

25. Open the vent valve connected to chamber gradually. You should hear the hissing sound to the point that it gets to the atmospheric pressure.

26. Now system is shut down and you can take your sample out.